

Sea level rise projections from storylines of Antarctic ice shelf collapse and its implication for adaptive planning in the Netherlands

In this study we model the dynamic sea level rise that results when Antarctica loses a substantial part of its buttressing ice shelves. To assess the timing of this loss, we perform a separate stability analysis that incorporates both oceanic and atmospheric forcings. We conclude that both the magnitude and the timing of larger scale sea level rise from Antarctic ice shelf collapse is principally controlled by the ocean-induced thinning but that atmospheric forcings have the ability to slightly expedite the moment of collapse. We further assess that larger scale ice shelf collapse is unlikely before the early second half of the 21st century, and that the resultant dynamic sea level rise will become important in the mid- to late second half of this same century. We find that the uncertainty caused by the variation between the ice sheet models is more than twice as large as the uncertainty caused by the triggers for ice shelf collapse. These findings suggest that if we want to better curtail the sea level rise uncertainty from a large dynamic contribution of the Antarctic Ice Sheet, curbing - or at least attributing - variations between ice sheet models is more important than the development of better predictions for the sub-shelf melting. We confirm that a long-term perspective on sea level rise can help policy makers to overcome decision paralysis on the short- to mid-term. Indeed, when Antarctic ice shelf collapse becomes a distinct possibility, it is likely not a matter of if and how to adapt to certain levels of sea level rise, but when to adapt. Flexible measures with a short lead- and lifetime can play a role in the adaptive strategy, but are inferior to larger measures for an extreme sea level rise scenario like the one considered here, or when taking on a long-term perspective.

1 Introduction

The ice sheet of Antarctica forms the largest frozen freshwater reservoir in the world, encompassing a sea level equivalent ice mass of more than 55m (Morlighem et al., 2020). It follows that the loss of even a small fraction of its mass could soon dominate future sea level rise (SLR), and the region has therefore received considerable attention from the international scientific community. Over the last decades, the SLR contribution from Antarctica has grown larger, and is indeed accelerating (IPCC, 2021). Previous research has shown that the primary control on this (accelerating) mass loss, is a weakening of the floating extensions of ice that are fringing the continent. These so-called ice shelves provide buttressing for the grounded ice mass of Antarctica, and their weakening leads to a retreat of the grounding line (GL) and a concomitant acceleration of the inland ice flow towards the sea (Pritchard et al., 2012).

Both the atmosphere and ocean can play a role in the weakening of the ice shelves. Ocean-induced melting at the base of the ice shelf draft, hereafter basal melt, is put forward as the

main cause for the observed mass losses in the Amundsen and Bellingshausen Sea areas, and the Aurora Subglacial basin (Sun et al., 2020). Modelling efforts and observations provide increasing evidence for a large sensitivity of the ice shelves in these sectors to a warming of the ocean (e.g., Gudmundsson et al., 2019), but there is still large uncertainty regarding the relation between the changing ocean temperatures and changes in sub-shelf melt (Jourdain et al., 2020). The ocean waters below the ice shelves are extremely difficult to reach, so that observational products are often infrequent, limited in space, and biased due to the mainly summertime sampling. Large variations in the modelled basal melt originate from our limited understanding of the physical processes at the ice-ocean draft, and the large variations between the different ice sheet models (Jourdain et al., 2020). In this context, Seroussi et al. (2019) point at the different numerical schemes, initialization procedures and physics that are in use between ice sheet models.

Basal melt may be the leading mechanism for Antarctic mass loss (Pritchard et al., 2012), atmospheric forcings can work alone or in tandem with the ocean to hasten the process of ice shelf weakening. For instance, previous research found that several major ice shelf disintegration events since 1995, including the Prince Gustav (1995), Larsen A (1995), Larsen B (2002) and Wilkins (2008) ice shelves, were ushered in by warmer periods with high melt that triggered melt water ponding and concomitant hydrofracturing (Scambos et al., 2009; Bell et al., 2018). These specific events occurred at or near the Antarctic Peninsula (AP) but the reported surface melt intensities and meltwater ponding are not unheard-of in other parts of Antarctica either. It raises the question if the events on the AP are indicative of future changes elsewhere on the continent when atmospheric conditions start to change.

From a policy perspective, the uncertainty on when, how much and how fast (future) SLR will take place, has a paralysing effect on decision making. Under deep uncertainty, policy makers are urged to take an adaptive approach that consists both of short-term, low-regret actions and pathways anticipating mid- to long-term options for SLR (Haasnoot et al., 2020). The adaptive plan of the Dutch Delta Program is currently benchmarked for a SLR range between 0.35 and 1m in 2100, but observed accelerations in SLR, as well as the formulation of physically plausible mechanisms of ice shelf collapse, have raised the concerns about an end-of-the-century SLR that is much higher. More so, there is an increasing awareness amongst policy makers that SLR must be anticipated for on the long-term because of the large inertia of the Greenland and Antarctic Ice Sheets. A long-term perspective means that higher levels of SLR need to be accounted for in the adaptive plan, which may help to overcome decision paralysis due to uncertainty. Using a long-term perspective, one might argue that for some decisions it is not a matter of *if* and *how* to adapt, but *when* to adapt (Slangen & Haasnoot, 2020). For a low-lying country like the Netherlands timely signals for adaptation are important to avoid lock-in situations where the only available option is to make large coastal defence reinforcements at exorbitant costs. It is therefore important to further reduce the SLR uncertainty from Antarctica under high-end warming scenarios, and develop early warning signals for a large contribution of the Antarctic Ice Sheet (AIS), so that adaptive

measures can be realised before it is too late.

Under the umbrella of the Coupled Model Intercomparison Project (CMIP6) from the Sixth Assessment Report (AR6), and as part of the Ice Sheet Model Intercomparison Project (ISMIP6), several experiments were designed to explore the uncertain Antarctic contribution to the global mean sea level (GMSL). One of these experiments is the ABUMIP-experiment, an acronym for the Antarctic BUttrressing Model Intercomparison Project. Sun et al. (2020) designed the experiment to investigate how changing ice shelves control Antarctic mass loss independent of the triggers for how and when ice shelves weaken. This unrealistic yet simple experiment allowed them to isolate uncertainties in response to a loss of buttressing between ice sheet models, whilst removing uncertainties related to the processes of ice shelf thinning and weakening. The experiment gauges the full SLR potential from Antarctic ice shelf collapse but is poorly constrained; the participating models predict a SLR anywhere between 1-12m over 500 years from now (Sun et al., 2020; Berends et al., 2022).

In this study, we seek to bring the ABUMIP-experiment and the triggers that cause ice shelf disintegration together. We use data on the modelled climate over the ice shelves, and on the melting at the ice shelf draft, to estimate how and when ice shelves could become unstable or lose their buttressing force. By means of a literature survey, we will put a threshold for conditional stability on the modelled climate over the ice shelves, as well as on the minimal thickness of the ice shelf, where it is assumed that thickness changes are mostly controlled by the basal melt (Pritchard et al., 2012). These efforts will result in a storyline of Antarctic ice shelf collapse that features the time and place of collapse of the different ice shelves bordering the continent. The loss of buttressing causes a dynamic response in the flow of the grounded ice - that we model - and results in a global mean SLR (GMSLR) projection for the continent. This sea level projection can be translated to a SLR at the Dutch coast, where it is compared to the design water levels and intended closing frequencies of the major storm surge barriers in the Netherlands. The sea level projections and associated storylines of ice shelf collapse can be used by adaptation planners to estimate the last possible moment in time when a decision on an adaptive measure may be taken, and to see if there are timely signposts in the data to signal these adaptation tipping points. By repeating this process for different stability criteria we can get an uncertainty estimate for the triggers of Antarctic ice shelf collapse. Our results complement those from the ABUMIP-experiment in the sense that we now have an estimate for the uncertainty from the ice-dynamical models and for the uncertainty from the triggers of ice shelf collapse.

In the following we will first elaborate on our methodology, and in particular on the setting of critical thresholds for ice shelf stability, to continue with a presentation of the results and a critical discussion. The discussion will pay special attention to the uncertainties in the methodology, and uses the discourse as a stepping stone for recommendations on follow-up research. The conclusion constitutes a brief overview of mainly the results and the discussion.

2 Material and Methods

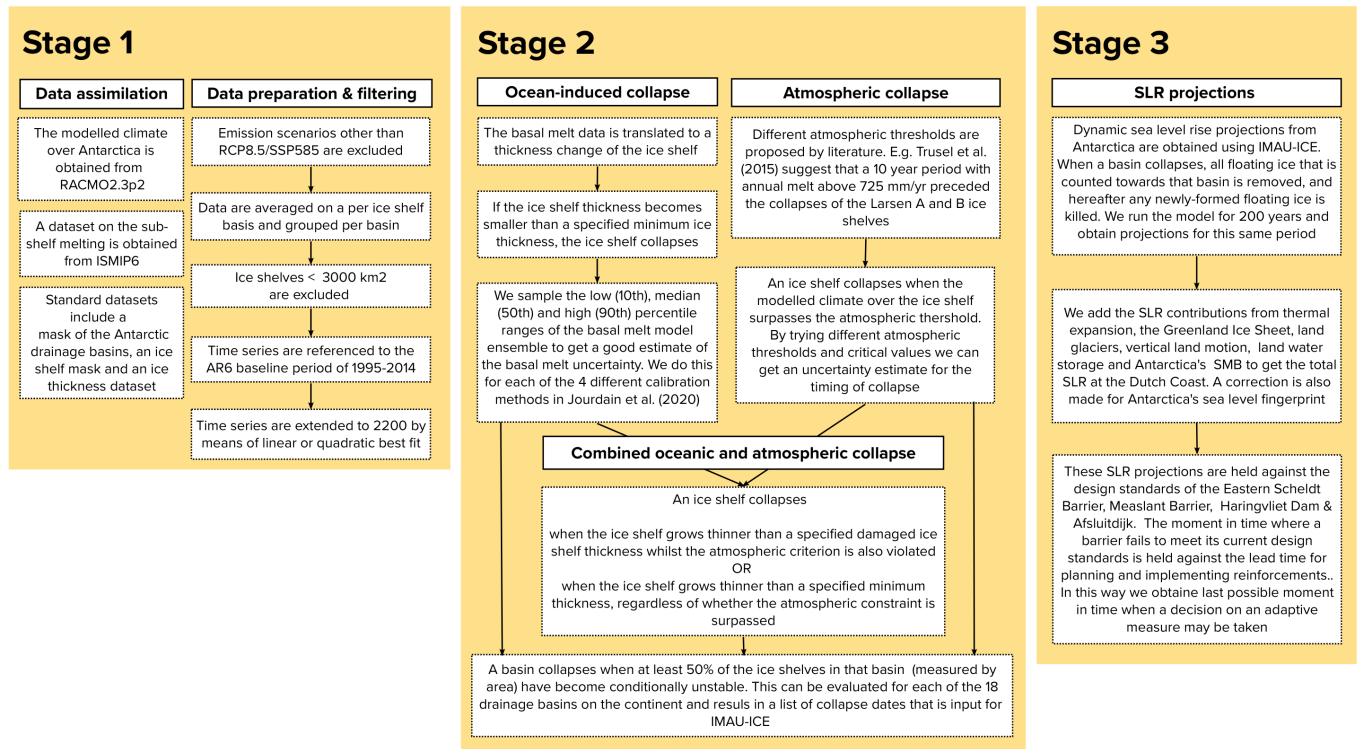


Figure 1: Overview of the Material and Methods

The following section describes the process of generating the sea level projections at the Dutch coast. In simple terms, the approach consists of the three largely independent stages depicted in Figure 1. The first stage is associated with the assimilation, preparation and filtering of the atmospheric and oceanic model data (Section 2.1). These data form the basis for our analysis and are used in the second stage to find out which ice shelves lose their buttressing force (Section 2.2). The atmospheric and oceanic datasets carry their own uncertainties but these are merely taken as a given and not or only marginally explored in this study.

The second stage tackles the issue of conditional ice shelf stability and the choice of related atmospheric and oceanic thresholds. This stage uses knowledge that is at the limits of our current understanding on the dynamics and stability of the AIS. This is reflected in the methodology used in this stage, which has an exploratory nature.

The third stage concerns the running of an ice-dynamic model named IMAU-ICE and returns the dynamic contribution of Antarctica to the GMSLR for the different collapse scenarios obtained from stage 2 (Section 2.3). This then has to be translated to a total SLR at the Dutch coast by adding e.g., the contributions from steric expansion and the Greenland Ice Sheet, whilst accounting for Antarctica's sea level fingerprint. That is, because the loss of

mass from Antarctica causes gravitational, rotational and short-term elastic responses of the Earth’s surface that modulate Antarctica’s SLR contribution regionally. In the following we will look at these three stages in more detail. In the last part of the method section (Section 2.4) we describe how the sea level projections may be used for adaptive SLR planning at the Dutch coast.

2.1 Data assimilation, preparation and filtering

If not already, all atmospheric and oceanic data is re-sampled to yearly data and referenced to the baseline period of 1995-2014 often used in AR6 climate projections. In due course the dataset is extended from 2100 up until 2200 (Section 2.1.4) because a threshold might be violated past 2100 for certain ice shelves and our interest is not limited to what happens in the 21st century only. Also, the ice-dynamic model needs to be run past 2100 if we want to adequately capture the dynamic response of the ice to an end-of-the-century loss of buttressing.

2.1.1 Atmospheric data

The atmospheric data used in this study originate from both historical and SSP585-forced simulations of different atmospheric variables generated by RACMO2.3p2. The original model output consists of monthly-averaged fields of e.g., near-surface temperature, snowmelt, snowfall and sublimation, averaged on a per ice shelf basis. Ice shelf definitions correspond to those used by the IMBIE2 team (Shepherd et al., 2018), and were first used by Rignot et al. (2011). The model ran at a horizontal resolution of 27km.

RACMO2.3p2 combines the dynamical core of the High Resolution Limited Area Model (HIRLAM 6.3.7), and the physics from the European Centre for Medium-Range Weather Forecast Integrated Forecast System physics (ECMWF-IFS, cycle CY33r1), for its modelling efforts. This version makes further use of a multilayer snow model that calculates melt, refreezing, percolation and runoff of meltwater, and a routine that simulates the interaction of near-surface air with drifting snow and the lower atmosphere. Moreover, RACMO2.3 makes use of an improved surface albedo scheme based on a predictive scheme for snow grain size and a background ice albedo prescribed by MODIS. Since RACMO is a regional model it utilises global input as forcing at its lateral boundaries and at the sea surface. In this case, the model is forced by 6-hourly CESM2 data from a SSP585 scenario. The reader is pointed at Van Wessem et al. (2018) for further information on the model performance.

2.1.2 Basal melt data

The basal melt projections used in this study are based on oceanic temperature & salinity fields from six CMIP5 global circulation models that ran a SSP585/RCP8.5 forcing scenario. More specifically, CCSM4, CSIRO-mk3-6-0, HadGEM2-ES, IPSL-CM5AMR, MIROC-ESM-CHEM, and NorESM1-M. The resolution of the CMIP5 models varies from a few tens to hundreds of kilometers, so that the ice shelf cavities of Antarctica and the circulation therein cannot be explicitly resolved (Stewart et al., 2018). However, the basal melt parameterization that will be explained shortly requires temperature and salinity fields underneath the ice shelves. For this reason, Jourdain et al. (2020) horizontally extrapolate the open ocean water properties from the observed climatology and CMIP5 into the ice shelf cavities. Also, they retain the vertical structure of the ocean temperature.

The parameterization that translates the extrapolated temperature and salinity fields into a melting at the ice shelf draft is the same for all models. Nonetheless, the variation between the CMIP5 models that is caused by the different oceanic temperature and salinity fields, and by the different numerics, physics etc., creates an uncertainty range for the sub-shelf melting. This uncertainty is sampled at the low (p10), mid (p50) and high (p90) percentile ranges to explore the effect of varying magnitudes of basal melt on the stability of the ice shelves.

The basal melt parameterization assumes a quadratic relationship between the basal melt and ocean thermal forcing. That is, because the melt rate linearly increases with the difference between the in-situ freezing temperature and the in-situ ambient ocean temperature (i.e. not modified by the buoyant plume), but is also modulated by the buoyancy-driven turbulent circulation at the ice shelf draft. Upon first approximation the latter increases linearly with the thermal forcing, so the basal melt increases with the thermal forcing squared. In an idealized study, Favier et al. (2019) demonstrated that this simple melt parameterization has similar skill at reproducing observed melt rates around Antarctica as more sophisticated parameterizations like e.g., Lazeroms et al. (2019), and Pelle et al. (2019). A more extensive intercomparison has recently been published by Burgard et al. (2022).

The parameterization depends on two coefficients that need tuning to produce meaningful results. To this extent, Jourdain et al. (2020) present two different calibrations that reproduce the mean observed basal melt rates across Antarctica (MeanAnt) or Pine Island Glacier (PIGL), respectively. Two slightly more complex variations that include a dependency on the local slope - as suggested by Little et al. (2009) and Jenkins et al. (2018) - are also provided. We note that the dataset imported for this study uses median estimates for the coefficients of the parameterizations and calibration methods. The data will therefore highlight the uncertainty in the sensitivity of melting to ocean warming but for experiments that all start from the median observed melt rates for Antarctica and Pine Island Glacier.

2.1.3 Standard datasets

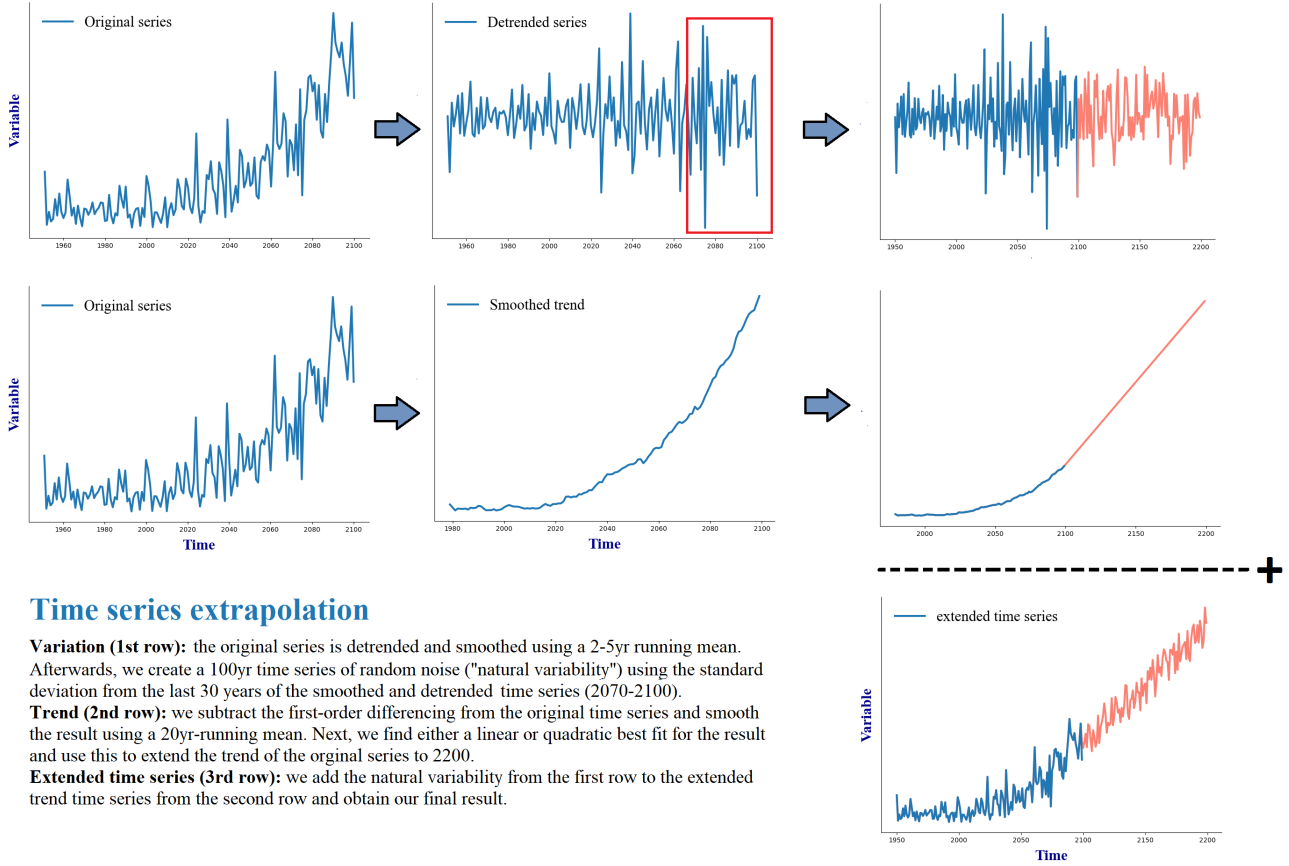
Several datasets are used in this study. Shapefiles for the ice shelves and drainage basins are obtained from Rignot et al. (2011). In their mappings, Antarctica is divided into 18 drainage basins that feed some 236 ice shelves of varying size. The basins map is extended to the surrounding Southern Ocean by means of a nearest neighbour search following Reese et al. (2018). This is needed because the GL and basin geometry can freely evolve over the runtime of the simulation, so that every grid point needs a basin tag which identifies to which drainage basin it belongs. For the purpose of linking atmospheric and oceanic effects on the ice shelf stability, a dataset of the ice shelf thickness is needed. Here we use the Bedmap2 ice thickness dataset from Fretwell et al. (2013). The mean thickness of the ice shelves is obtained by grouping the floating ice grid points from the Bedmap2 dataset on a per ice shelf basis using the shapefiles from Rignot et al. (2011), and averaging the result.

2.1.4 Data preparation and filtering

Some basins and ice shelves are excluded from the analysis because they are too small in size. This is merely a model constraint imposed by the resolution of RACMO, as ice shelves must appear larger than the model resolution to be featured, and must have enough grid points to minimize erroneous results from averaging on a per ice shelf basis. Indeed, when you erroneously include an ocean grid point in your shelf mask, you don't want it to impact the results too much. Here we impose the condition that the ice shelf area needs to be larger than 3000 km², corresponding to at least 4 grid points at the 27km resolution of the RACMO data. All ice shelves that pass this criterion are listed in Figure 6. Basin 12 is fully excluded from the analysis because all its fringing ice shelves are too small, but according to Figure 7 this should not impact the final SLR projections too much. There is at least one listed ice shelf in every other basin.

The gridded basal melt data from Jourdain et al. (2020) are averaged on a per ice shelf basis. This is convenient because the atmospheric data are also provided in this format (Section 2.1.1). We will reflect on the implications of using shelf-mean melt rates rather than e.g., melt rates at the GL, in Section 4.1.

The atmospheric and oceanic (basal melt) data are extended from 2100 to 2200 because a threshold might be violated past 2100 for certain ice shelves and our interest is not limited to what happens in the 21st century only. The extrapolation procedure is described in Figure 2.



Time series extrapolation

Variation (1st row): the original series is detrended and smoothed using a 2-5yr running mean. Afterwards, we create a 100yr time series of random noise ("natural variability") using the standard deviation from the last 30 years of the smoothed and detrended time series (2070-2100).
Trend (2nd row): we subtract the first-order differencing from the original time series and smooth the result using a 20yr-running mean. Next, we find either a linear or quadratic best fit for the result and use this to extend the trend of the original series to 2200.
Extended time series (3rd row): we add the natural variability from the first row to the extended trend time series from the second row and obtain our final result.

Figure 2: The different steps of the time series extrapolation

2.2 Threshold setting

2.2.1 Atmospheric threshold setting

The apparent linkage between atmospheric conditions and the viability of ice shelves (Section 1) has led several authors to try and find atmospheric thresholds for ice shelf stability of varying complexity. In this study we investigate three thresholds from literature, namely:

1. The proposed threshold of Morris & Vaughan (2003). They noticed that the ice shelves which have retreated since the early 1900s all lie between the -9°C and -5°C isotherms, where the present limit is well-approximated by the -9°C annual isotherm. It is therefore hypothesized that the current climate-controlled limit of viability for ice shelves is well-approximated by this -9°C isotherm. The atmospheric stability condition then becomes that the N-year running mean surpasses a temperature threshold of $X^{\circ}\text{C}$, where N and X are varied around the -9°C reported by Morris & Vaughan (2003) to investigate the

robustness of the threshold. In this case, we set N to 5 years and vary X between -10°C and -8°C .

2. Trusel et al. (2015) noted that a 10-consecutive-year period with annual melt above $725 \text{ mm w.e. yr}^{-1}$ preceded the collapses of the Larsen A and B ice shelves on the AP. The atmospheric stability condition then becomes that the N-year running mean surpasses a snowmelt threshold of $X \text{ mm yr}^{-1}$, where N and X are varied around the $725 \text{ mm w.e. yr}^{-1}$ reported by Trusel et al. (2015) to investigate the robustness of the threshold. In this case, we set N to 10 years and vary X between 650 and 800 mm w.e. yr^{-1} .
3. Pfeffer et al. (1991) introduced a simple model that relates the transient processes of infiltration, refreezing and runoff in the snowpack. In the process they suggested that a melt over accumulation ratio (MoA) larger than 0.7 is prognostic for the onset of melt-water ponding and surface water runoff. Meltwater can deepen crevasses and cause flexural stresses, leading to hydrofracturing and ice shelf destabilization (Kuipers Munneke et al., 2014; Spergel et al., 2021). The MoA may thus be interpreted as a threshold for conditional ice shelf stability too. The MoA used in this study is calculated as follows:

$$MoA = \frac{\text{melt}}{\text{accumulation}} = \frac{\text{snowmelt} + \text{rainfall}}{\text{snowfall} + \text{sublimation}} \quad (1)$$

The atmospheric stability condition then becomes that the N-year running mean surpasses a MoA-ratio of X, where N and X are varied around the 0.7 (-) value reported by Pfeffer et al. (1991) to sample its robustness. In the this case we set N to 5 years and vary X between 0.6 (-) and 0.8 (-).

Modelled quantities like the snowfall, snowmelt, temperature and rainfall may vary a lot between years and per location. To make sure that these thresholds are not surpassed by full coincidence but are rather symptomatic of broader long-term change, we take the running mean of these quantities. However, one cannot ex ante rule out the possibility that a series of (isolated) events weaken the ice shelf to a point where it disintegrates - e.g., three consecutive summers with unusually high melt can deteriorate the ice to a point where it breaks up - even though the long-term running mean is not exceptionally high. We therefore make a modification to the second condition and designate it the "Trusel interannual (-)"-condition:

4. Ice shelves collapse when the annual melt reaches above $X \text{ mm w.e. yr}^{-1}$ for K times in N years, where X, K and N are varied to sample the condition's robustness. In the Trusel interannual case we set N to 5 years, K to 3x and vary X between 650 mm w.e. yr^{-1} and 800 mm w.e. yr^{-1} .

As a standalone condition (that is, not considering the ice thickness or basal melt, see 2.2.2), the year where the aforementioned thresholds are exceeded for the first time marks the

collapse date of the respective ice shelf. The collapse date of the entire basin is determined from the collapse dates of the individual ice shelves that are considered part of that basin using the procedure outlined in Figure 3.

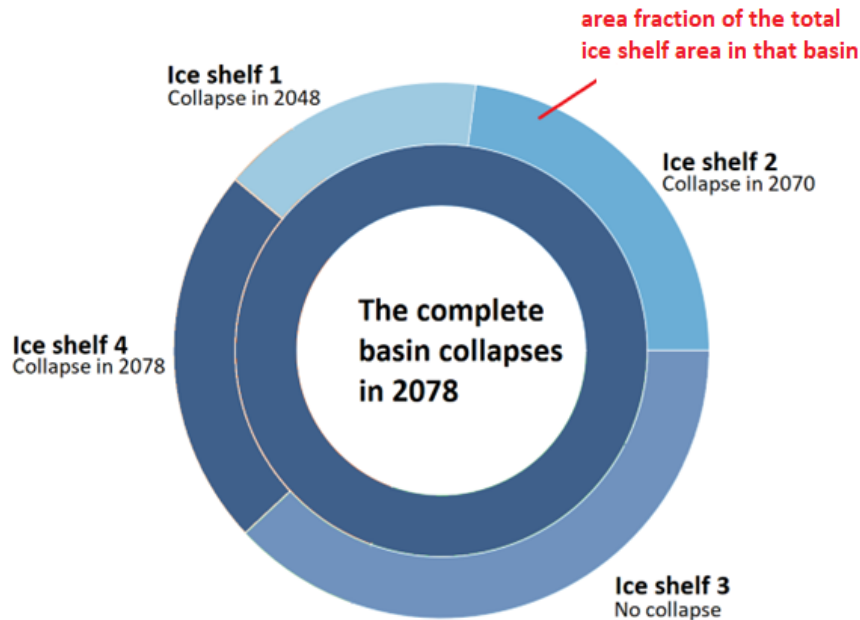


Figure 3: Setting the timing of basin collapse. The complete basin collapses when the threshold condition is passed for more than 50% of the ice shelves in that basin, as measured by the area sum. In the case depicted here, this is true when ice shelves 1,2 *and* 4 have collapsed. The implications of using a threshold of e.g., 30% or 80% were only marginally explored. For the basins that are made up of one big ice shelf it makes no difference. The largest differences were found for basins that consist of 2 or 3 larger ice shelves (e.g., basin 13 & 15 from Figure 6). Even so, this is an artifact over our choice to average the model data on a per ice shelf basis and can be avoided as will be discussed in Section 4.

2.2.2 Setting a threshold for the basal melt through the ice thickness

As mentioned in Section 1), the mass loss projections from sub-shelf melting are not well constrained, and in large part this may be attributed to uncertainties associated with (the parameterization of) sub-shelf melting (IPCC, 2021), and the large variations between different ice sheet models. The basal melt data from the ISMIP6 reflect this uncertainty, so that we can try different percentiles ("scenarios") to get a complete picture on how the basal melt uncertainty impacts the timing of collapse (Section 2.1.2). One important consequence of the sub-shelf melting is that the ice shelf becomes thinner. If the ice shelf grows thinner it also becomes weaker, and more frequent break-up events from e.g., tidal flexure, may be expected (Massom et al., 2018). It is therefore that we want to translate to sub-shelf melting

to a thickness change of the ice shelf for our stability analysis. Hereto we use the following formula:

$$Hi(t + \Delta t) = Hi(t) + dSMB(\Delta t) + dBMB(\Delta t), \quad (2)$$

where $Hi(t+\Delta t)$ is the updated ice shelf thickness, $Hi(0)$ is the present-day ice shelf thickness from Bedmap2, and $dSMB$ and $dBMB$ are the anomalous surface mass balance (RACMO2.3p2) and the anomalous basal melt (Jourdain et al., 2020), respectively. Ice shelves are in an assumed steady state with the SMB and BMB from the 1995-2014 reference period, so that anomalies and offspring thickness changes are defined relative to this baseline. A thinning of the ice shelf will likely cause a change in the ice flux over the GL. However, we assume that the timescale leading to a change in the GL flux from this loss of buttressing is longer than the timescale of passing the ice thickness threshold for collapse. By extension this implies that we assume the flux to be constant in time.

As a standalone condition (that is, not including atmospheric forcings), the year where the ice shelf grows thinner than a minimal ice shelf thickness of 200m marks the collapse date of that ice shelf. This is a mere observational constraint as there are currently (almost) no larger ice shelves in Antarctica that have an overall ice thickness below the 200m (Fretwell et al., 2013). Again, the collapse date of the entire basin is determined using the approach outlined in Figure 3.

2.2.3 Integrating atmospheric and oceanic thresholds for ice shelf collapse

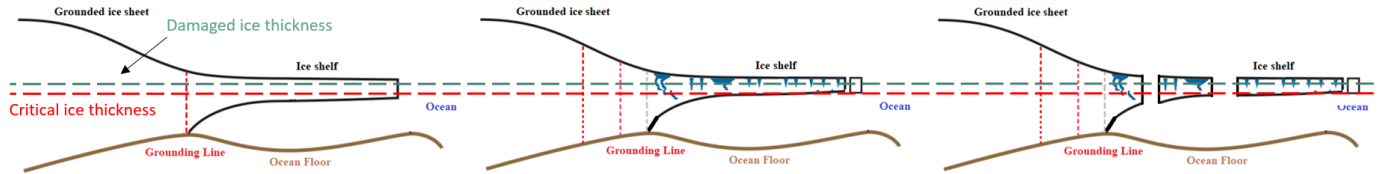
The atmospheric and oceanic thresholds can be integrated through the concept of a minimal "damaged" ice thickness, alongside the idea of a critical ice thickness. Ice that shows little crevassing and open fractures can support larger yield stresses and is less receptive to disintegration. Yet damaged ice can carry less weight and breaks up at an earlier stage (Bassis & Walker, 2012).

Conceptually, the critical ice thickness is the minimum ice thickness that the ice shelf can have to just support its own weight. If the overall thickness of the ice sheet grows thinner than this minimal ice thickness, we impose the condition that it breaks down. Again, we use a thickness of 200m for this critical ice thickness.

The minimal "damaged" ice thickness is the minimum ice thickness that an already damaged ice shelf can have if it still wants to support its own weight. By damage we mean that the ice is crevassed, features open fractures or is damaged in any other manner that compromises the maximum stresses that the ice can withstand. The damaged ice thickness is always larger than the critical ice thickness. If the overall thickness of the ice sheet grows thinner than this damaged ice thickness, it breaks down on the condition that the imposed atmospheric threshold is also exceeded. E.g., the ice shelf collapses if the ice thickness becomes less than 250m, whilst the 5yr-running mean of the temperature lies above the -9°C isotherm. Figure

4 shows how the concepts of a "damaged" and "critical" ice thickness can be used to combine the forcing effects of the ocean & atmosphere.

An ice shelf collapses when it grows thinner than a specified *damaged* ice thickness of e.g., 250m, whilst the atmospheric collapse criterion is also violated



OR when it grows thinner than a specified *critical* ice thickness of e.g., 200m

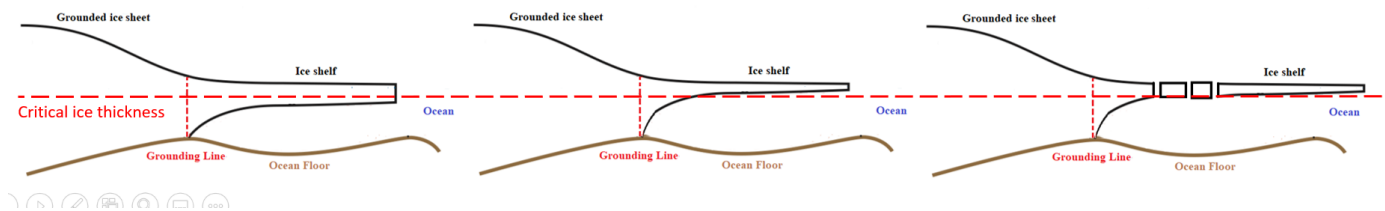


Figure 4: Schematic explaining the integration of the atmospheric and oceanic thresholds through the concept of a damaged and critical ice thickness.

In reality, the point at which an ice shelf breaks down under its own weight is also dependent on factors like size, the location where this damage occurs, and the amount of support that is provided by its surroundings (e.g. neighbouring walls can offload stresses). The approach should therefore be regarded as a simple first order approximation of what constitutes a non-durable (damaged) ice shelf thickness.

2.3 Sea level rise projections

2.3.1 IMAU-ICE

IMAU-ICE v2.0 is an ice sheet model that simulates the flow of ice through solving the englacial velocity and temperature fields, and is used in this study to simulate the future extent and sea level contribution of Antarctica. The englacial velocity field is solved using the "depth-integrated viscosity approximation" (DIVA) of the stress balance that was first derived by Goldberg (2011). This higher-order stress approximation includes both vertical and longitudinal shear stresses, plus the stresses due to longitudinal stretching caused by vertical shearing. The approximation is computationally efficient and agrees well with other higher-order approximations and the full Stokes equations down to spatial scales as small as

10km (Pattyn et al., 2008; Schoof & Hindmarsh, 2010). The evolving ice sheet geometry is determined by integrating the mass conservation equation. The temperature field is solved in three dimensions using a discretized version of the heat equation that is described in detail in Berends et al. (2021). The model makes further use of Glen’s flow law, where the temperature-dependent flow factor is linked to the englacial temperature field using an exponential Arrhenius relation (Huybrechts, 1992).

Sliding is modelled using a regularised Coulomb-type sliding law (Pattyn et al., 2017), where the till friction angle and basal yield stress are calculated following Martin et al. (2011).

In order to accurately capture the GL motion due to the sub-shelf melting, IMAU-ICE v2.0 makes use of an approach that scales the basal friction term near the GL with the square of the sub-grid grounded fraction. A similar parameterization was adopted before by the PISM and CISM models (Feldmann et al., 2014; Leguy et al., 2021), and it improved their numerical stability and relaxed some of the resolution requirements for accurately reproducing the GL motion. Berends et al. (2022) have reported similar effects for IMAU-ICE. IMAU-ICE has different options when it comes to the modelling of the sub-shelf melting. However, in this study we set the basal mass balance to zero everywhere, which is akin to saying that we eliminate the effect that sub-shelf melting has on the dynamics of the GL. We will provide a rationale for this choice in Section 4.2.

Climate and SMB forcings are prescribed by RACMO2.3 and fixed at present-day values (Van Wessem et al., 2014). A spatially variable but temporally constant geothermal heat flux is prescribed based on the data from Shapiro & Ritzwoller (2004). Calving is parameterized by a simple threshold-thickness calving law, with a default threshold thickness of 200m.

More information on the model can be found in Berends et al. (2022).

2.3.2 Model initialization

In this study, we run IMAU-ICE at a 40km resolution. Model spin-up was realised in two steps. First, the model is initialized with the observed present-day geometry from the Bedmachine Antarctica v1.0 dataset (Morlighem et al., 2019) and englacial temperatures according to the Robin solution. Second, after a 100 year relaxation the ice dynamic component of the model was switched off and the model was run for the duration of 240 kyr (i.e. several glacial-interglacial cycles) to reach thermal equilibrium at present-day conditions.

Unfortunately, an initialization of IMAU-ICE that captures both the present-day ice sheet geometry and is in steady state, is not yet realized (Figure S6). In part, this may be attributed to a deep uncertainty surrounding the correct tuning of such parameters as the rheology of the ice and the basal friction at the ice-bedrock interface, caused by a lack of observations. The IMAU-ICE modelling group is currently working on a better initialization for the model but these efforts come too late for us. Regardless, the problem was circumvented by subtracting the control run from every model result.

2.3.3 Removal of ice shelves in IMAU-ICE

In the original ABUMIP-experiment from Sun et al. (2020) two different methods to implement the Antarctic ice shelf collapse are considered. The ABUK-variant removes all ice shelves at the start of the simulation, and thereafter any newly-formed floating ice is instantaneously removed ('float-killed'). That is to say, at all times, the calving flux is assumed to be larger than the flux across the GL to prohibit regrowth of the shelves. The ABUM-variant applied an extreme sub-shelf melting rate that inevitably led to a rapid loss of ice shelves. We take an approach that is similar to the one used in the ABUMIP-ABUK experiment except that we do not remove all floating ice at once and at the start of the model run. Instead we use the results from the threshold analysis to make a list of the different collapse dates of the 18 Antarctic basins from Rignot et al. (2011). This list is then used to float-kill the ice shelves in the different basins at their respective basin collapse dates during model runtime. See Section 4.3 for a rationale on why we have chosen the ABUK-approach over the ABUM-approach.

2.3.4 Coping with model-related uncertainties

Factors like the model initialization method, numerical scheme, ice dynamics (e.g., sliding law, stress balance equation), grid resolution and included physics (e.g., type of calving, hydrofracturing, maximum cliff height) have a significant impact on the model results (e.g., Seroussi et al., 2019). The ABUMIP-experiment from Sun et al. (2020) sampled this uncertainty for a scenario of Antarctic ice shelf collapse and concluded that the resulting spread is indeed very large. Since we do not seek to repeat this study - or to make a model sensitivity study from IMAU-ICE - we keep the model settings constant between runs. Differences between model runs are then caused by the prescribed differences in the spatial and temporal signature of conditional collapse, and allow us to sample the uncertain timing of Antarctic ice shelf collapse due to its triggers. We assume that the uncertainty arising from the forcing of the ice shelf collapse is larger than the uncertainty arising from the ice dynamics itself when the model parameters are kept constant. In Section 4.5 we compare the model uncertainty estimate from Sun et al. (2020) with our uncertainty estimate from the triggers of ice shelf collapse.

2.3.5 Translating sea level curves to sea level projections at the Dutch coast

IMAU-ICE calculates the ice-dynamic contribution of Antarctica to the GMSLR. However, this contribution still needs to be translated to a SLR at the Dutch coast. First, the result needs correction for the sea level fingerprint of Antarctica; mass loss from Antarctica impacts the Geoid as the redistribution of water also implies a redistribution of mass. At the Dutch coast the cumulative outcome of these gravitational, rotational and deformation effects is a SLR that is larger than the rise in GMSL alone (Mitrovica et al., 2009; Hay et al., 2014). These effects are impromptu accounted for by multiplying the sea level curves with a fac-

tor of 1.25 (Hay et al., 2014). Also, the results are augmented with the other components of SLR, specifically, the SLR caused by thermal expansion and changing wind and ocean circulation patterns ('sterodynamic effects'), the Greenland Ice Sheet, land glaciers, vertical land motion, and land water storage. These numbers are obtained from the NASA Sea Level Projection Tool ([website](#)) that utilises AR6 sea level projection data. Data are available for different scenarios, confidence levels and percentiles but here we use the median values of the SSP585 scenario that are assigned medium confidence.

Dynamic losses in West Antarctica are being partially offset by increases in snow accumulation over East Antarctica (Kittel et al., 2021). To account for this, the future SMB of Antarctica was obtained from the RACMO2.3p2 data and added to the total sea level curve. In summary, to obtain the total SLR at the Dutch Coast we use IPCC-values for the non-Antarctic components, RACMO for the SMB of Antarctica and IMAU-ICE for the dynamic component of Antarctica.

2.4 Adaptive planning for sea level rise

To assess the timing of adaptation, both the lifetime of decisions and the time required for planning and implementing (follow-up) measures is important. Here we use the modelled sea level contributions from Antarctica to assess when the Dutch storm surge barriers 'fail' to meet the original design standards of the Dutch Delta Program. Large defence structures typically have the longest (follow-up) lead times and highest design standards in terms of safety and functional lifetime, so that they are arguably the most complicated and critical elements of a durable adaptive strategy. It is therefore that we choose to focus on the larger coastal defence barriers of the Netherlands, specifically the Eastern Scheldt Barrier, Maeslant Barrier, Afsluitdijk and Haringvliet Dam. To evaluate their performance, we use the same proxies as Haasnoot et al. (2020), namely (a) the closure frequency as a proxy for impacts on safety, ecology and navigation; and (b) the exceedance frequencies of design water levels as a proxy for the failure of the barrier. Data is obtained from this same publication and shown in Figure 5. The closing frequency and violation of the closing criteria are assessed for the Eastern Scheldt and the Maeslant storm surge barriers. The return period of exceedance of the design water levels is examined for all the barriers.

In Section 2.3 we discussed how the results from the stability analysis (Section 2.2) are translated to a range of sea level projections at the Dutch Coast. This SLR projection range is held against the design standards of the different barriers to estimate the moments in time when the barrier fails to meet its current design standards. When augmented with the time that is needed to plan and implement for a reinforcement of the barrier ("lead time"), we find the so-called adaptation tipping point. The adaptation tipping point indicates the last possible moment in time when a decision on an adaptive measure may be taken (Haasnoot et al., 2020).

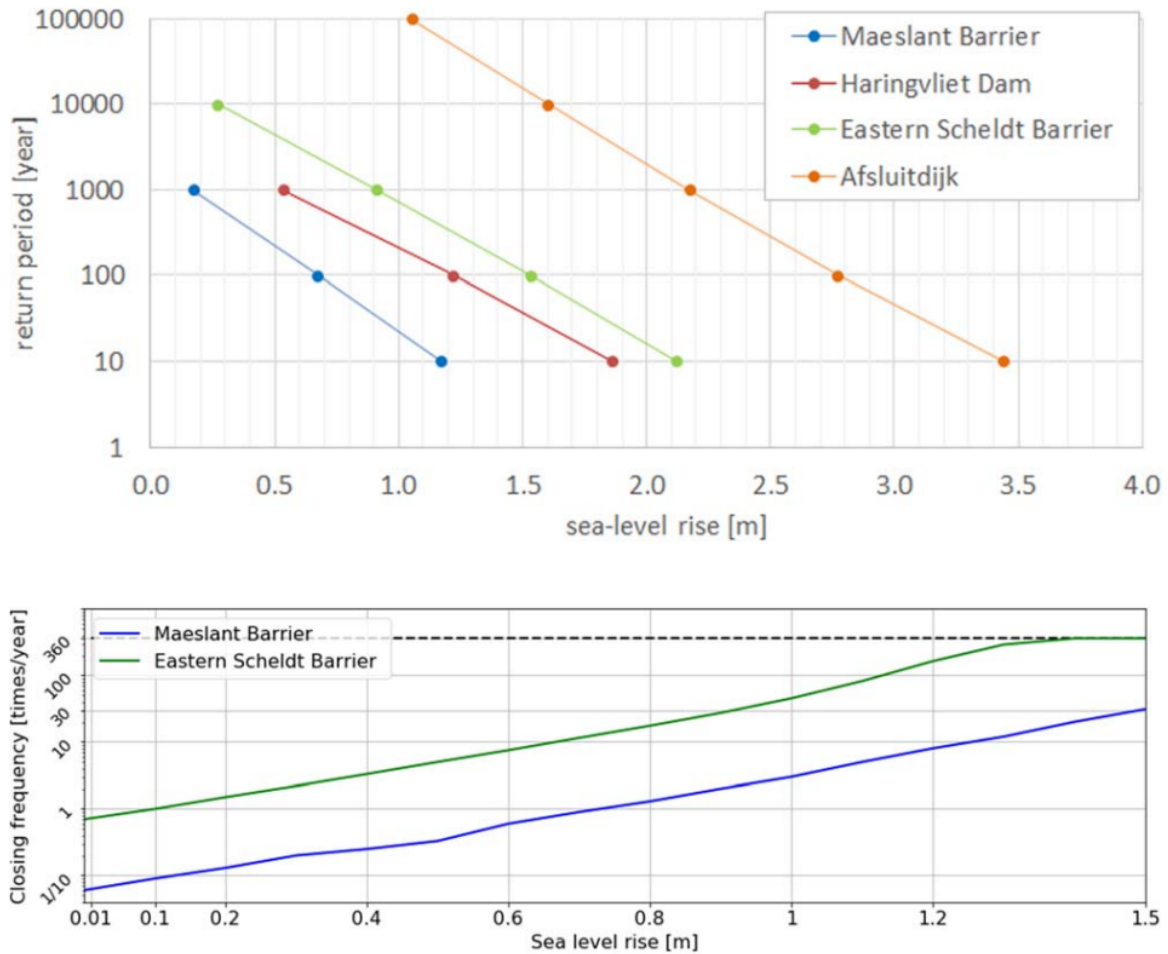


Figure 5: Top: return period of exceedance of the design water levels for the Maeslant Barrier, Haringvliet Dam, Eastern Scheldt Barrier and Afsluitdijk. **Bottom:** closing frequency of the Maeslant Barrier and the Eastern Scheldt Barrier for different SLR levels, assuming present-day closure criteria. These figures are taken directly from Haasnoot et al. (2020).

A timely signpost for the failure of the barrier would then constitute any signal (e.g., basin collapse, an acceleration of the sea level) that manifests itself before an adaptation tipping point. Ideally these signposts have discriminatory value, i.e. they rule out certain possibilities for the future sea level evolution.

3 Results

Figure 6 lists all 36 ice shelves that are included in the analysis and indicates the basin number that they are assigned to. These basin numbers are used in the text and in the figures and are thus important to understand the result section.

Basin	Ice shelf	Fraction of total shelf area in basin	Present-day ice thickness
1	Brunt_Stancomb	0.43	205m
1	Riiser-Larsen	0.47	302m
1	Ekstrom	0.06	357m
2	Filchner	1	846m
3	Ronne	1	639m
4	LarsenD	0.83	138m
5	George_VI	0.32	286m
5	LarsenC	0.59	293m
5	Bach	0.06	235m
6	Stange	0.46	202m
6	Wilkins	0.5	155m
7	Abbot	0.84	237m
8	Pine_Island	0.25	458m
8	Crosson	0.17	376m
8	Dotson	0.29	500m
8	Cosgrove	0.17	314m
9	Nickerson	0.08	211m
9	Getz	0.8	464m
10	Ross_West	0.95	440m
10	Sulzberger	0.04	367m
11	Ross_East	1	372m
13	Mertz	0.38	463m
13	Cook	0.31	321m
14	Totten	0.36	875m
14	Holmes	0.18	372m
14	Moscow_University	0.36	769m
15	Shackleton	0.56	257m
15	West	0.32	332m
16	Amery	1	598m
17	Prince_Harald	0.54	193m
18	Jelbart	0.1	436m
18	Nivl	0.06	311m
18	Fimbul	0.32	294m
18	Lazarev	0.06	244m
18	Baudouin	0.27	266m
18	Borchgrevink	0.18	336m

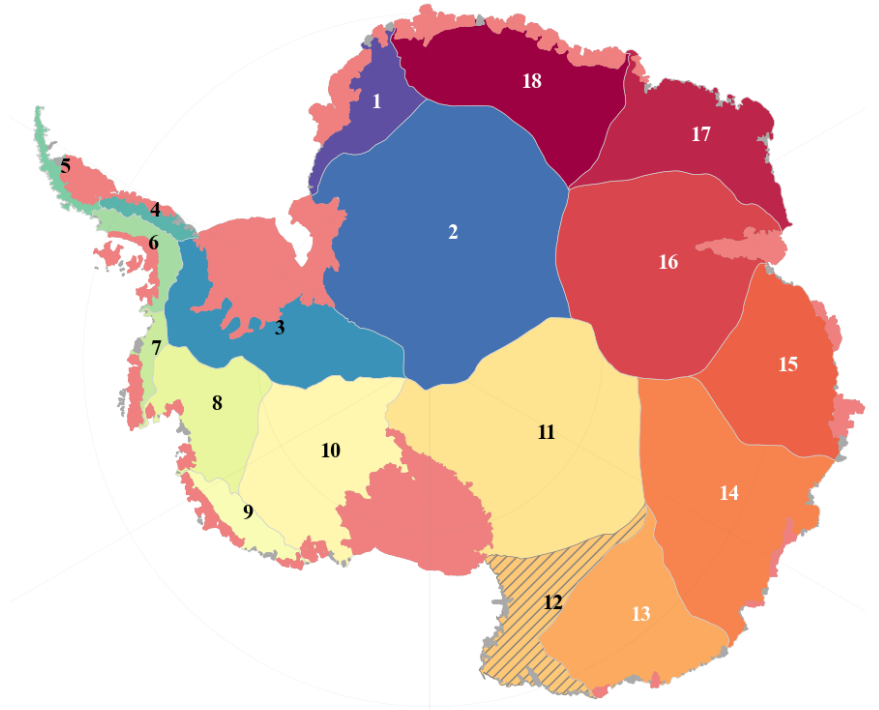


Figure 6: *Left:* table of ice shelves that are included in the analysis, the corresponding basin, the fractional area of the ice shelf w.r.t. the total ice shelf area in that basin, and the present-day average ice thickness. *Right:* Geometry of the different Antarctic basins from Rignot et al. (2011), and the associated basin reference number and color coding that will be used in subsequent figures. In pink the ice shelves that are included in the analysis. Basin 12 is not included in the analysis because all its adjoining ice shelves are smaller than 3000 km².

3.1 Sea level rise potential of the different Antarctic basins

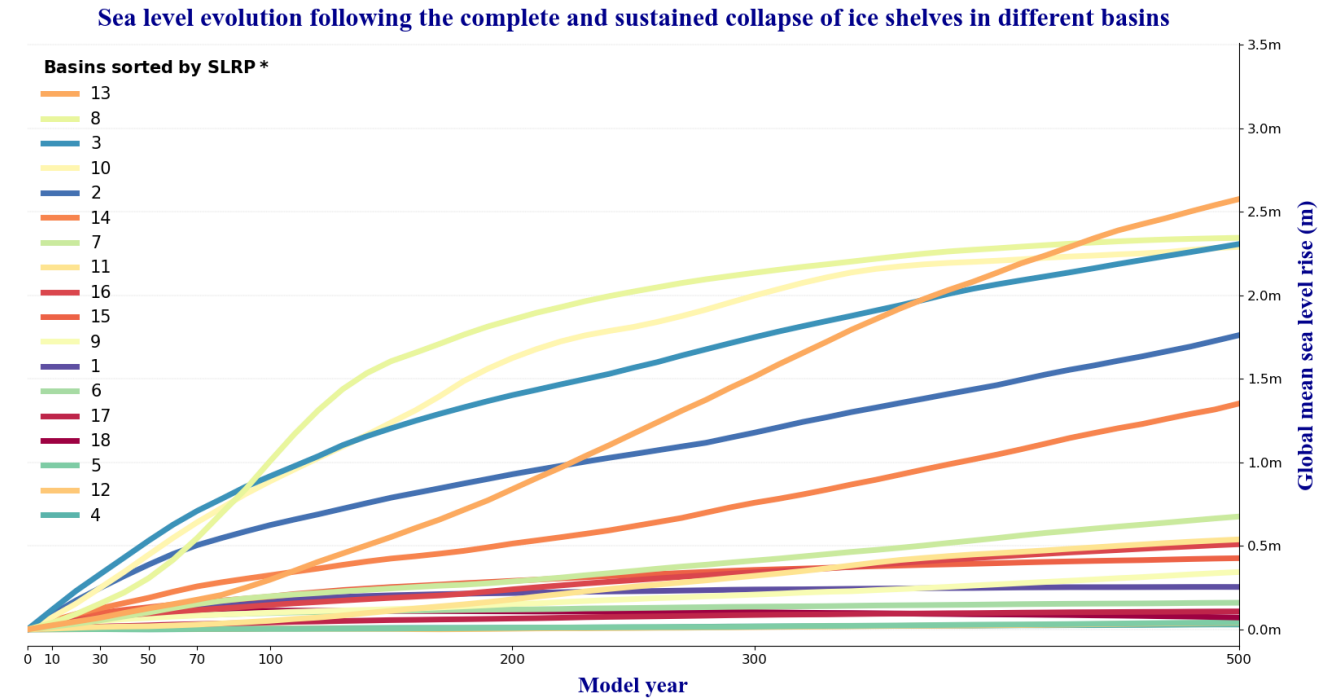


Figure 7: SLR Potential (SLRP) of the different Antarctic basins from Rignot et al. (2011). Line colors correspond to the basin reference colors from Figure 6.

Figure 7 gives an estimate of the maximum dynamic contribution of the individual Antarctic basins over a 500 year time period. We refer to this contribution as the sea level rise potential (SLRP) of that basin. The SLRP of the individual basins is obtained from IMAU-ICE by removing all the ice shelves counted to that basin at the start of the model run, float-killing any newly-formed ice, and running the model forward for 500 years.

The largest dynamic contributions originate from a loss of grounded ice mass in the Admundsen Sea Sector (basins 7 & 8), the Wilkes Subglacial Basin (basin 13), and the Aurora Subglacial Basin (basin 14), and from a collapse of the Ross and Filchner-Ronne ice shelves (respective basins 10, 2 & 3). Put differently, these basins now buttress a relative large share of the grounded ice mass of Antarctica, and their collapse would cause a significant rise in the GMSL.

For most basins, the rate of mass loss is highest for the first 100-200 years but there are cases (e.g., basin 13 & 14) where mass loss rates remain high for the full 500yr period and beyond. The initial rapid SLR, subsequent flattening, and final concurrence of the different SLRPs from basin 3, 8 & 10 hint not only at an almost complete loss of the West AIS (WAIS), but also signal at a cascading effect where the collapse of one basin heralds the collapse of the next. Note that when the draining of ice starts to change the initial drainage divides, and ice

is exchanged between adjacent basins, the SLR contribution from the individual basins can be different from the sum of their SLRPs. This effect is implicitly captured in the ice-dynamic model.

3.2 SLR from Antarctic ice shelf collapse under the combined influence of the ocean and atmosphere

Unless stated otherwise, the p50 of the basal melt model ensemble is discussed, as well as a SSP585 forcing scenario.

3.2.1 Magnitude of the dynamic SLR contribution from Antarctica

Figure 8 shows the evolution of the GMSL for the different (combinations of) oceanic and atmospheric thresholds used in this study. The scenario that combines the oceanic & atmospheric constraints (top panel, blue shading) projects a dynamic SLR contribution from Antarctica anywhere between 0.18-1.23m by 2100, and 3.69-5.36m by 2200. However, there exist large differences between the different calibration methods (bottom panel); The MeanAnt calibrations project a SLR between 3.69-3.90m by 2200, whereas the PIGL calibrations project a SLR between 4.60-5.36m. The PIGL estimates are therefore considerably higher than the MeanAnt estimates, and also give a larger uncertainty range. The p10 and p90 of the basal melt model ensemble give a lower and upper bound for the SLR projections from the combined ocean & atmosphere of 0.02m (1.63m) and 3.02 (5.91m) by 2100 (2200), respectively (top panel, orange shading).

3.2.2 Primary control on the dynamic SLR contribution from Antarctica

The SLR projection bandwidth that combines the influence of the ocean & atmosphere has significant overlap with the SLR projection bandwidth from the p50 of the ocean-only (top panel, green shading). However, the upper and lower bounds of the uncertainty range from the combined ocean & atmosphere is slightly shifted upwards relative to the upper and lower bounds of the ocean-only. In other words, the SLR is largely controlled by the basal melt but atmospheric forcings have the ability to slightly expedite the moment of collapse, leading to a (marginally) higher SLR. This same shifting effect is observed for the uncertainty range spanned by the p10 and p90 of the combined ocean & atmosphere, and the p10-p90 uncertainty range spanned by the ocean-only SLR pathway (not shown). The shift is most pronounced for the lower bounds of the uncertainty ranges as a lower basal melt favours a more decisive role for atmosphere-driven ice shelf weakening.

The SLR uncertainty bandwidth from the sole use of atmospheric constraints (top panel, red shading or Figure S1) largely disappears (bottom panel, bandwidth of the individual colored strips) when the conditional instability of the ice shelves is tied to both the exceedence of the atmospheric threshold and the notion of a minimal damaged ice thickness. Apparently, the

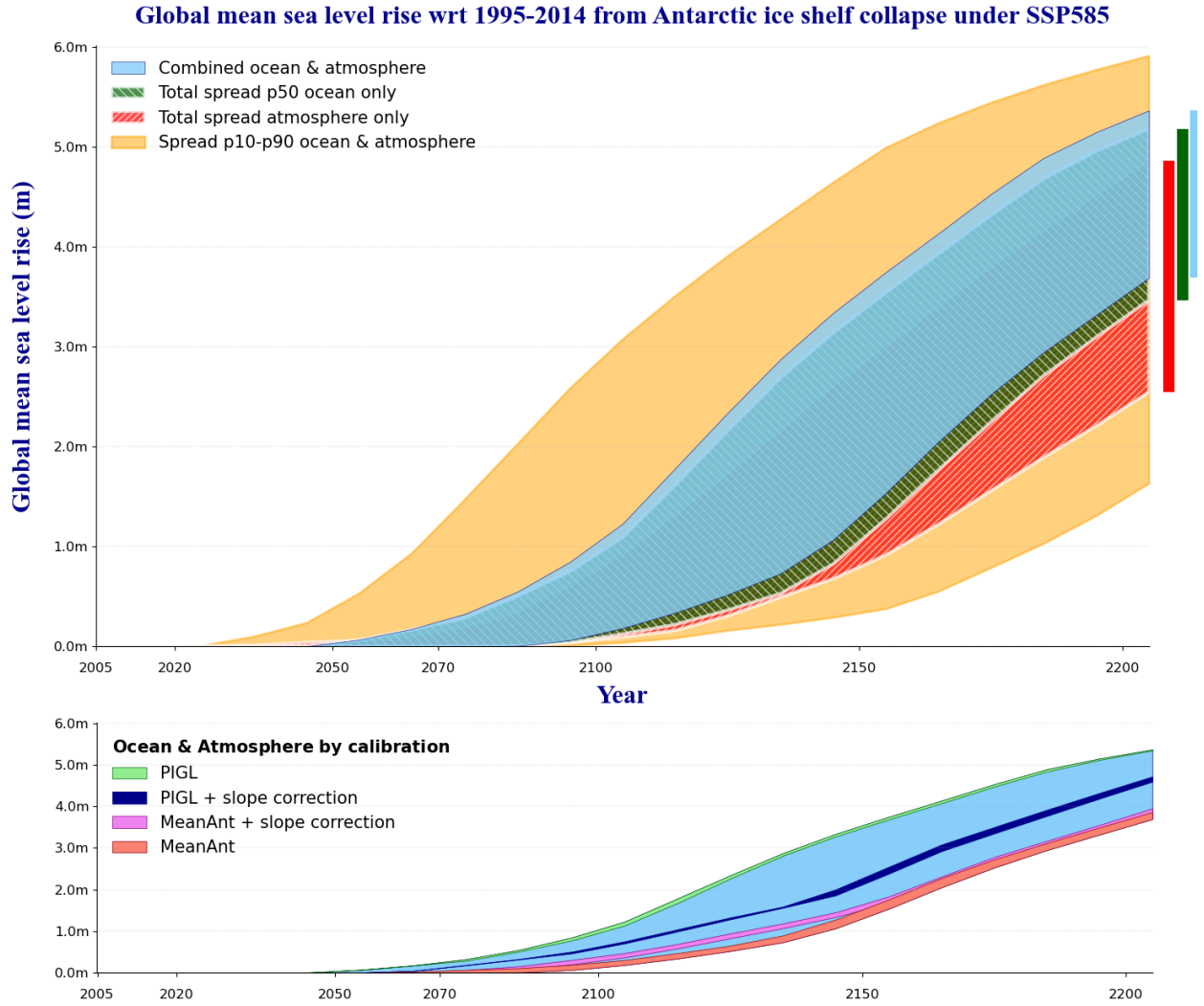


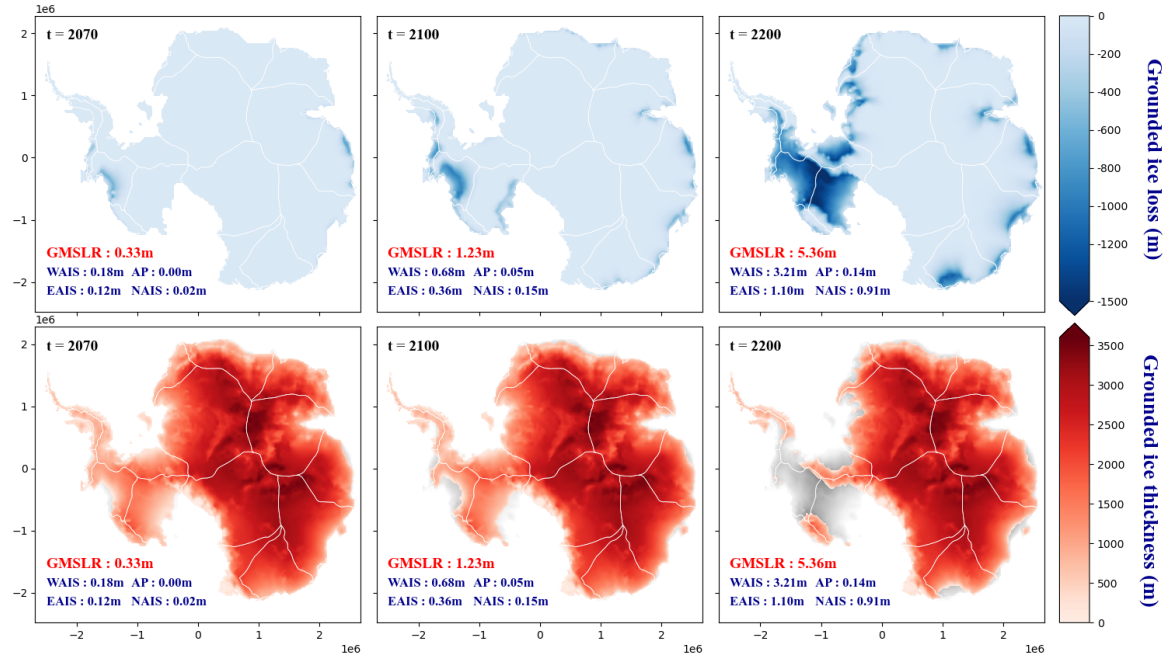
Figure 8: GMSLR w.r.t. 1995-2014 following the successive collapse of different Antarctic basins under a SSP585-forcing pathway. **Top:** In blue the spread in SLR from an approach that combines both atmospheric and oceanic constraints. We used the p50 of the basal melt model ensemble. An ice shelf collapses when it grows thinner than 200m *or* when the ice shelf grows thinner than 250m whilst the atmospheric criterion is also violated. In red the SLR spread when only using atmospheric constraints (see also Figure S1). In green the spread between the different basal melt calibrations using only the p50 of the basal melt model ensemble and assuming a 200m critical ice thickness (see also Figure 12). In orange the uncertainty range from the combined ocean & atmosphere sampling the p10 and p90 of the basal melt model ensemble. **Bottom:** SLR spread from the combined ocean & atmosphere using the p50 of the basal melt model ensemble. Each colored strip marks the SLR uncertainty between the most conservative (Trusel 650 mm w.e. yr⁻¹, Figure S1) and most pessimistic (Pfeffer 0.6, Figure S1) atmospheric constraint, whereas the different colors correspond to the different basal melt calibrations.

thickness constraint has a strong regulating effect on the timing of collapse of the different ice shelves, and by extension narrows the uncertainty bandwidth for the projected SLR. This is an important constraint for the collapse of the large ice shelves: it implies that if you have a thick ice shelf like e.g., the Filchner-Ronne, the ice shelf does not immediately collapse when the atmospheric criterion is violated, because there is still enough pristine ice beneath the damaged surface layer that prevents breakup.

3.2.3 Spatial patterns

The spatial patterns of mass loss between the highest (Pfeffer 0.6 + PIGL) and lowest (Trusel 650 mm w.e. yr⁻¹ + MeanAnt) threshold/calibration combinations are largely similar (Figure 9). In both scenarios, the WAIS is (almost) completely lost by 2200, with a GMSLR totalling 0.07-0.68m by 2100, and 2.5-3.2m by 2200. The contribution from the AP is only marginal, consistent with the low SLRP of the region (Figure 7). Before 2100, SLR from the North AIS (NAIS) largely comes from basins 16 and 18. In the second half of the next century basin 2 also start to contribute to the total of the NAIS. By 2200 the dynamic contribution of the NAIS adds up to 0.57-0.91m and judging from the SLRP of basin 2 (Figure 7) this mass loss will uphold for a long time past 2200. For the East AIS (EAIS) basin 15 is the largest contributor to the GMSLR up to 2100. However, by 2200 ice is also drained from basin 13 (Trusel + MeanAnt) and basins 13 & 14 (Pfeffer + PIGL), again signalling at a long and sustained draining of ice from that region far beyond 2200 (Figure 7). For the p90 and p10 of the combined SLR projections (orange shading, top panel Figure 8) the most important difference is that the WAIS has not (yet?) collapsed in the latter case (see Figure S2 for more detail).

Grounded ice thickness change (m) wrt 1995-2014 under SSP85 using Pfeffer and the PIGL calibration



Grounded ice thickness change (m) wrt 1995-2014 under SSP85 using Trusel and the MeanAnt calibration

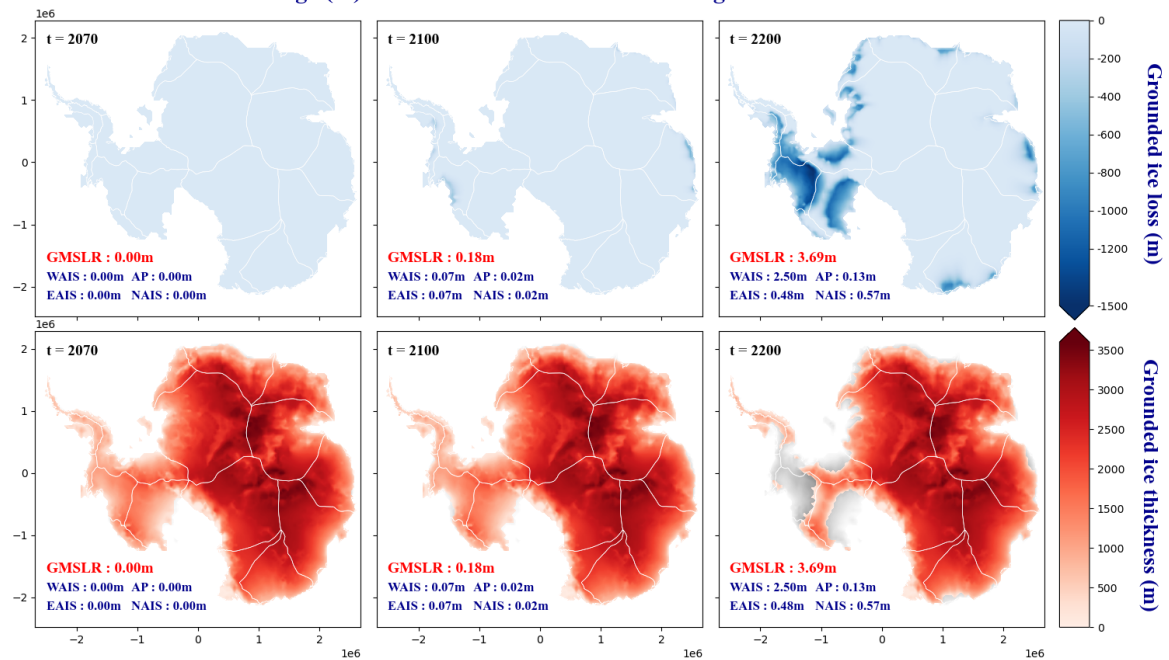


Figure 9: Loss of ice mass above flotation (blue panels) and the absolute thickness change (red panels) for the upper (two top panels) and lower (two bottom panels) bounds of the SLR uncertainty from the combined influence of the ocean & atmosphere, and the p50 of the basal melt model ensemble (Figure 8). WAIS: basins 3 & 7-11; EAIS: basins 13-15, AP: basins 4-6, NAIS: basins 1,2 & 16-18.

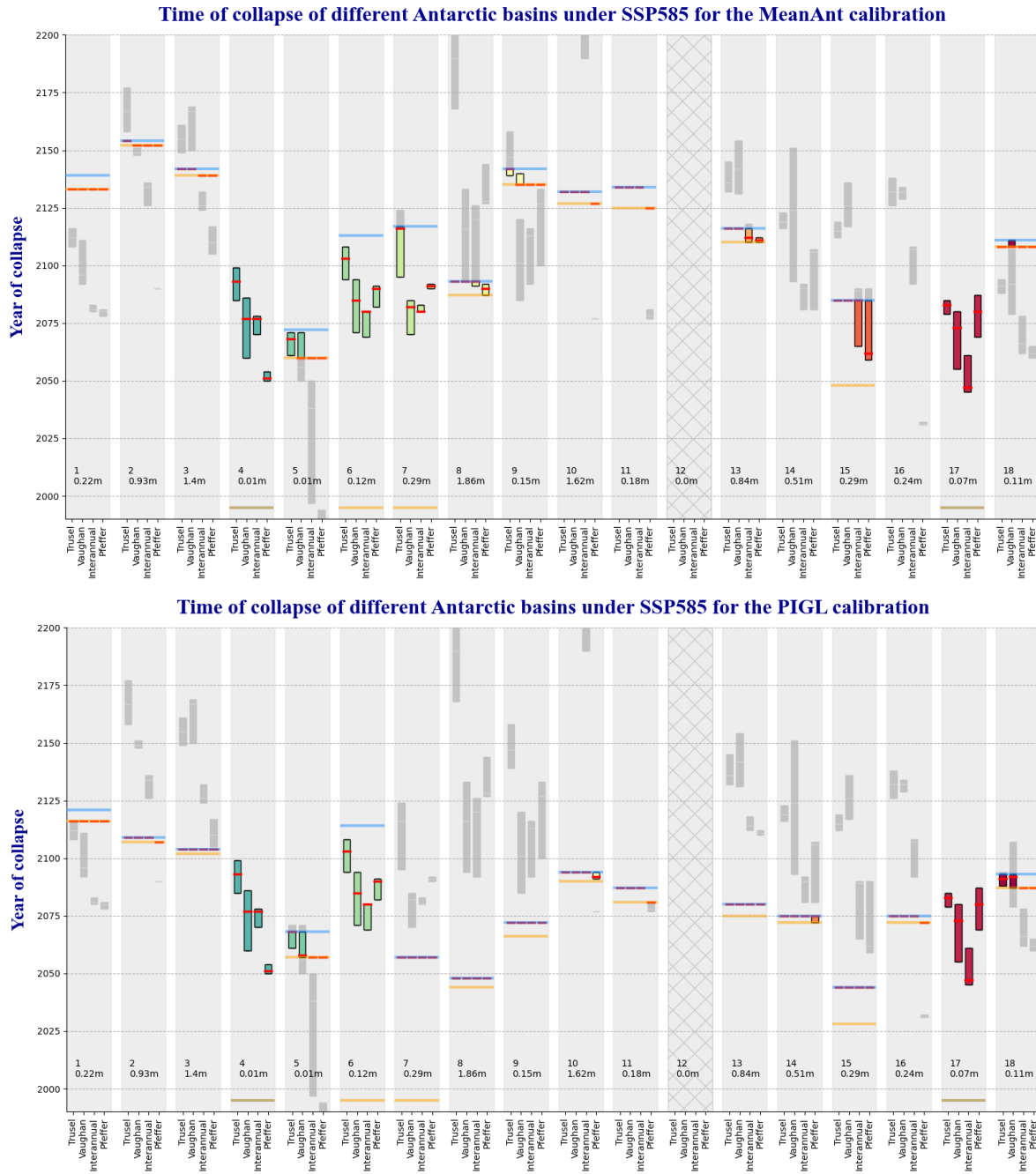


Figure 10: Time of collapse of the Antarctic basins under SSP585 for the different atmospheric thresholds, a 5-year running mean filter, and the MeanAnt (top) and PIGL (bottom) calibrations (data from the bottom panel of Figure 8). Blue lines stipulate the time when the ice shelf grows thinner than the critical ice thickness of 200m. Orange lines indicate the damaged ice shelf thickness of 250m. Grey and colored bars indicate the uncertainty in the timing of collapse from using only atmospheric constraints. These uncertainty bars are obtained by varying the atmospheric thresholds between 650 & 800 mm w.e. yr^{-1} for Trusel (Interannual), -10°C & -8°C for Vaughan, and 0.6 & 0.8 for Pfeffer. Bars are colored when they are placed in between the orange and blue line. In that case, the value of the atmospheric threshold plays a decisive role in the timing of collapse because the damaged ice thickness is reached and the atmospheric thresholds are violated before reaching the critical ice thickness of 200m. Grey bars indicate that either the damaged ice thickness acts as a controlling factor over the timing of collapse or the critical ice thickness is reached before the atmospheric constraints are violated. Ice shelves from basin 4 and 17 are already thinner than 200m from the start, but as they still exist today we impose the condition that they collapse the moment that the atmospheric threshold is exceeded. Numbers 1-18 correspond to the different basins from Figure 6. Plotted below the basin number is the SLRP for that basin at $t = 200$ (from Figure 7). Basin 12 was excluded from the analysis as all its adjoining ice shelves are smaller than 3000 km^2 .

3.2.4 Timing of basin collapse

For the p50 of the basal melt model ensemble, the dynamic contribution from Antarctica becomes significant in the early to mid second half of the 21st century, depending on the calibration method used. For the p90 of the basal melt ensemble this point lies around 2030 and for the p10 past 2100. The timing of collapse of the different basins for the different atmospheric thresholds and the most (least) conservative MeanAnt (PIGL) calibration is shown in Figure 10. The atmospheric thresholds play a decisive role in the timing of collapse for the AP region (basins 4,5,6) and for basin 17. For the MeanAnt calibration the collapse of basin 7 and 15 is also dependent on the choice for an atmospheric threshold. However, according to Figure 7 the total SLRP of these basins is relatively small when compared to the SLRP of the basins that are controlled by the principally ocean-induced ice shelf thinning. For the group of basins that have a high SLRP and collapse within the 200 year modelled period (basins 2,3, 8, 10 and 13), the timing between reaching the damaged ice thickness and critical ice thickness is typically on the order of ~ 10 years or less. Notwithstanding the uncertainty in the adopted methodology, this indicates that there is little manoeuvring space for the atmosphere to play a decisive role in regulating the dynamic SLR contribution from Antarctica for a scenario as in Figure 8. We conclude that not only the magnitude but also the timing of larger scale SLR is mostly controlled by ice shelf collapse from ocean-induced thinning. By looking at the congruence between the grey and orange dotted lines in Figure 8 we can anticipate that this conclusion also holds for the p90 of the combined ocean & atmosphere projections, but is less conclusive for the p10 of the basal melt ensemble.

3.2.5 Sensitivity to the magnitude of the ocean-induced basal melt

So far we concluded that - outside of the AP - the time and place of Antarctic ice shelf collapse is largely controlled by the ocean-induced thinning of the ice shelves. It is therefore important to further explore the uncertainty in the ocean part of the methodology. Here, one of the largest uncertainties is caused by the choice for a basal melt scenario from the total model ensemble. Figure 11 shows the time of collapse of the different Antarctic basins using different percentiles of the basal melt model ensemble, and not imposing any atmospheric constraints (for the atmospheric uncertainty, see Figure S3). One observes that the spread in the timing of collapse is very large (see also Table S4) Basins 1-3, 5 and 8 show a relative good agreement on the timing of collapse between the different calibration methods except for the PIGL calibration. For all these basins, but in particular basins 1-3, the PIGL calibration gives a much broader range for the timing of collapse for both the low and high percentiles of the basal melt model ensemble. Apparently, the ice sheet models have an increased sensitivity for the PIGL calibration in this region (approx. the Wedell Sea Region) that enlarges the intermodel spread. From the basins with a SLRP of more than 0.5m by 2200, basin 8 is likely to go first, followed by either one of basin 13 and 14 and finally by basins 2 and 3.

Time of collapse of different Antarctic basins under SSP585 using only oceanic forcings

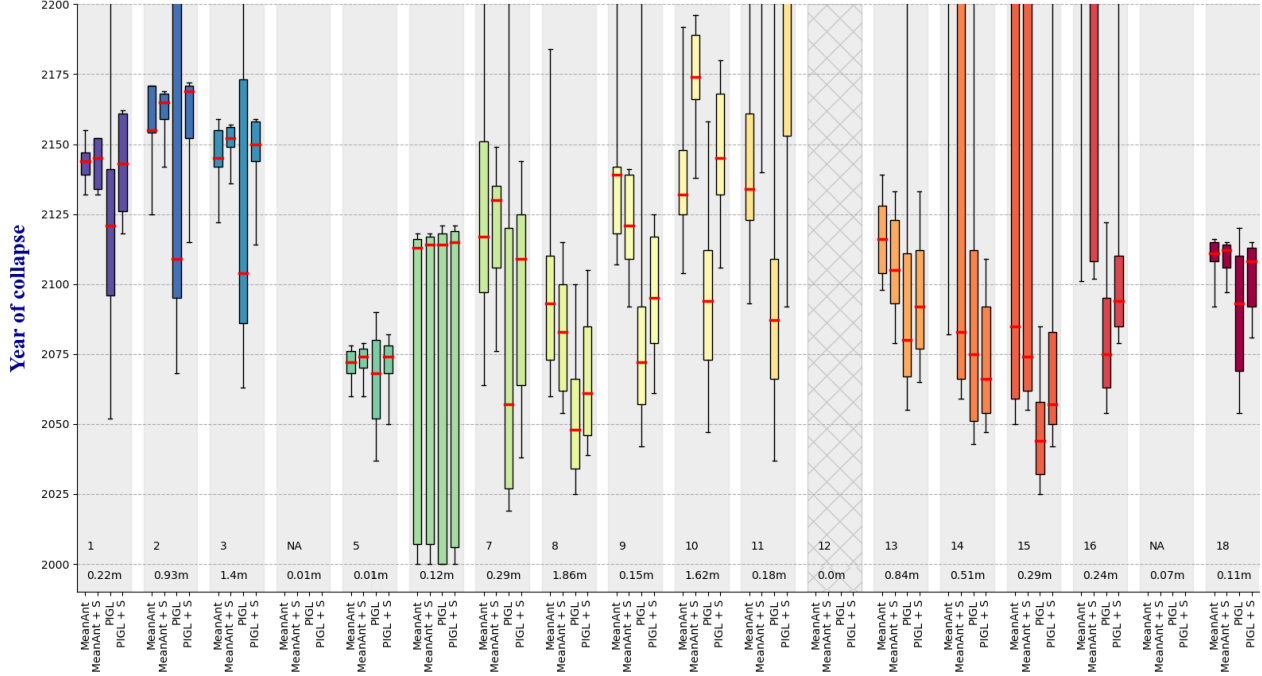


Figure 11: Time of collapse of different Antarctic basins under SSP585 using different percentiles for the basal melt, and not imposing atmospheric constraints. Shown for each basin is the uncertainty in the timing of collapse using a 200m critical thickness for the four different basal melt calibrations. As usual, each boxplot consists of an upper and lower whisker, first and third quartile, and median (red) corresponding to the p10, p90, p25, p75, and p50 of the basal melt ensemble, respectively. Basins 4 and 17 are not accessed (NA) because the thickness of the included ice shelves from these basins is already smaller than 200m at present. Plotted below the basin number is the SLRP for that basin at $t = 200$ (from Figure 7). Basin 12 is excluded from the analysis because all its bordering ice shelves are smaller than 3000 km².

Either way, large scale basin collapse outside of the AP is not to be expected before the second half of the 21st century, except for the worst case scenario (p90 with PIGL calibration).

However, the most important conclusion is that the intermodel disagreement on the (magnitude of) future basal melt needs to be much better constrained if we want to gain more insight in the possible timing of Antarctic ice shelf collapse. As several authors have pointed out before (e.g. Seroussi et al., 2019; Sun et al., 2020, this means that we need to work on both our physical understanding of the processes at the ice-ocean draft, and on curbing the variation between the different ice sheet models caused by e.g. the different numerical schemes, resolutions and initialization procedures.

The uncertainty from Figure 11 is also reflected in Figure 12. The difference between the upper and lower bound of the total SLR uncertainty range broadens from about 2.9m by 2100

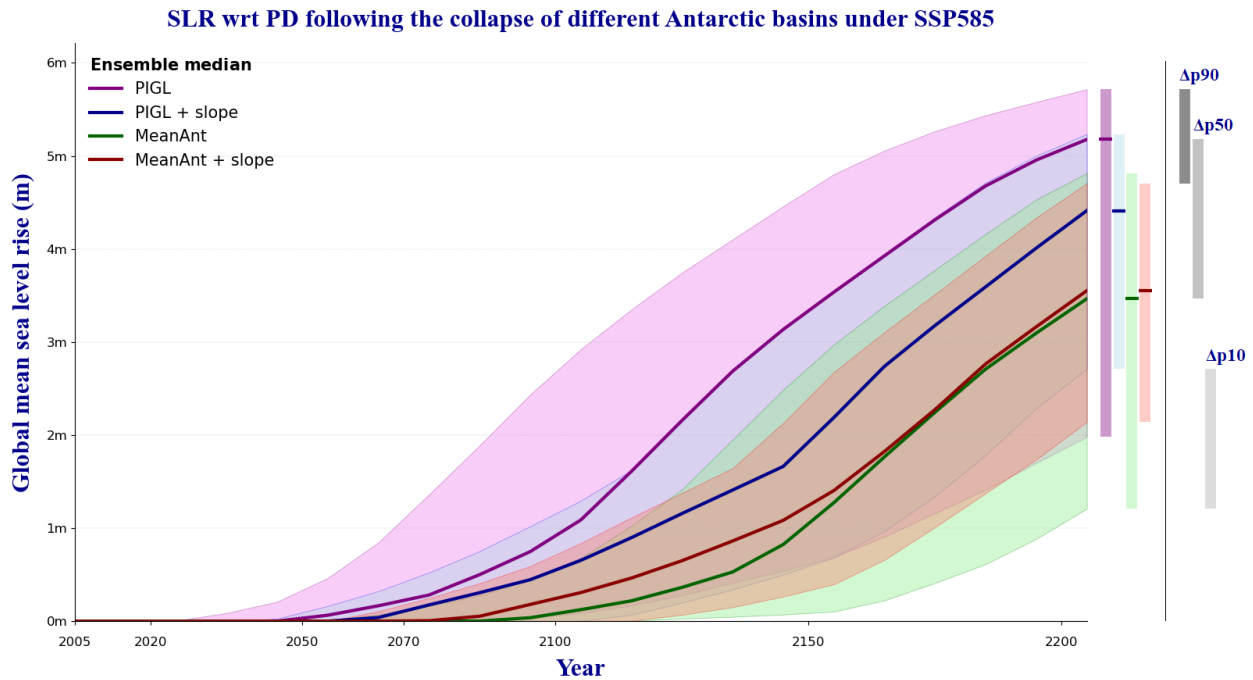


Figure 12: GMSLR w.r.t. 1995-2014 following the successive collapse of different Antarctic basins under a SSP585-forcing pathway using thickness changes from only the basal melt to estimate the timing of collapse. Ice shelves are assumed to collapse when the ice shelf grows thinner than 200m. In color the spread in the GMSLR between the p10 and p90 of the basal melt model ensemble for the different calibrations. Solid lines show the SLR pathway that follows from the median value of the basal melt ensemble. In grey tones the final spread between the distinct calibration methods but for the same basal melt percentile.

to more than 4.5m by 2200. The spread in the basal melt model ensemble (colored bars) is about 2x larger than the spread caused by the use of the different calibration methods but for the same percentile of the model ensemble, namely 1.4m versus 3.1m on average.

The MeanAnt calibrations project a smaller SLR than the PIGL calibrations for the p50 of the basal melt model ensemble (colored lines). The PIGL calibrations project a SLR between 5.18-4.41m by 2200, whereas the MeanAnt calibrations stick with a SLR of approximately 3.5m. The calibration methods that use a slope correction have a smaller SLR uncertainty bandwidth than the calibration methods that do not. This difference is about 1-1.2m. All together, the uncertainty from the choice of either the MeanAnt or PIGL calibrations is about as large as the uncertainty from the choice for a slope correction or not.

Returning to the uncertainties caused by the choice for a calibration method (grey bars), we make two more observations:

1. This uncertainty is larger for the p10 of the model ensemble than for the p90 by about 0.5m.

- The projection bandwidths of the p50 and p90 of the basal melt model ensemble show significant overlap, whereas the p10 has no overlap with the p50. As a consequence the mid-value of the p50 uncertainty range is about 85cm higher than the mid-value of 3.45m from the total uncertainty range. In other words, the full range of SLR projections is slightly skewed towards higher levels of SLR, likely because a loss of buttressing from either basin 8 or 10 leads to an inevitable loss of a large part of the WAIS (Figure 7).

In Section 4.1 we will reflect on the causes for the large projected differences between the PIGL and MeanAnt calibrations.

3.2.6 Timing of Adaptation tipping points

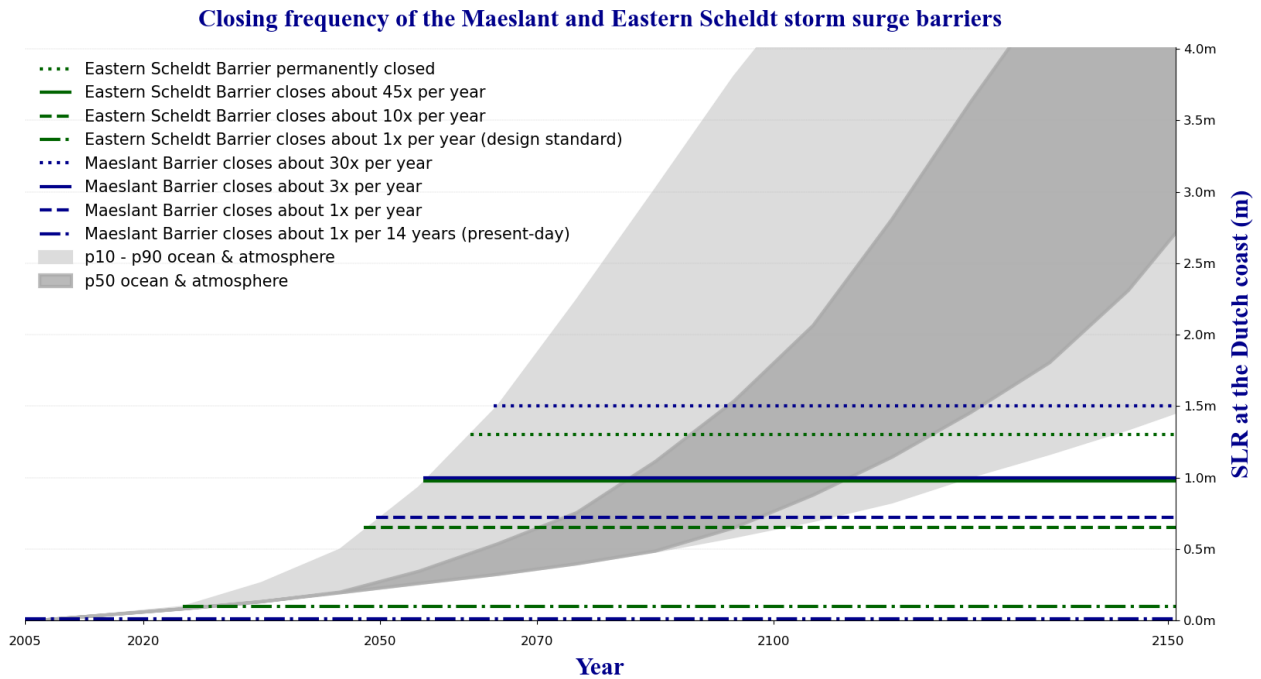


Figure 13: SLR at the Dutch coast w.r.t. 1995-2014 following the successive collapse of different Antarctic basins under a SSP585-forcing scenario. Horizontal lines indicate how SLR impacts the closing frequency of the Eastern Scheldt Barrier and Maeslant Barrier. In grey the maximum p10-p90 uncertainty range for the combined oceanic and atmospheric collapse criteria. In darkgrey the p50 for the combined ocean & atmosphere.

The Eastern Scheldt and the Maeslant storm surge barriers are key structures in the coastal defence system of the Netherlands. For most of the time the Eastern Scheldt barrier is open to preserve the ecology of the region and for the local shellfish farming. Likewise, the Maeslant Barrier is kept open to allow for navigation to and from the Inner Port of Rotterdam.

However, during extreme water events these barriers are closed. Under the current closure criteria, the Eastern Scheldt barrier is closed about once a year and the Maeslant Barrier is closed about once every 15 years. When the sea level rises the barriers will close more often, so that there is a higher probability of failing, navigation is hampered and ecology and local fishery are compromised. A closure of the Maeslant Barrier thereby obstructs a large part of the outflow of the Rhine River, which will increase flood risk along the rivers.

The Eastern Scheldt Barrier, designed to close on average once per year, would close 45x per year at 1m, and almost permanently at 1.3m of SLR, if the current closure criteria were maintained. The Maeslant barrier would close about 3x per year at a rise of 1m and about 30x per year for a SLR of 1.5m. In the latter case the navigation to and from the Inner Port of Rotterdam would be impeded during many weeks in the storm season (Haasnoot et al., 2020).

Exceedence probability of the design water levels (DWL) of the major storm surge barriers in the Netherlands

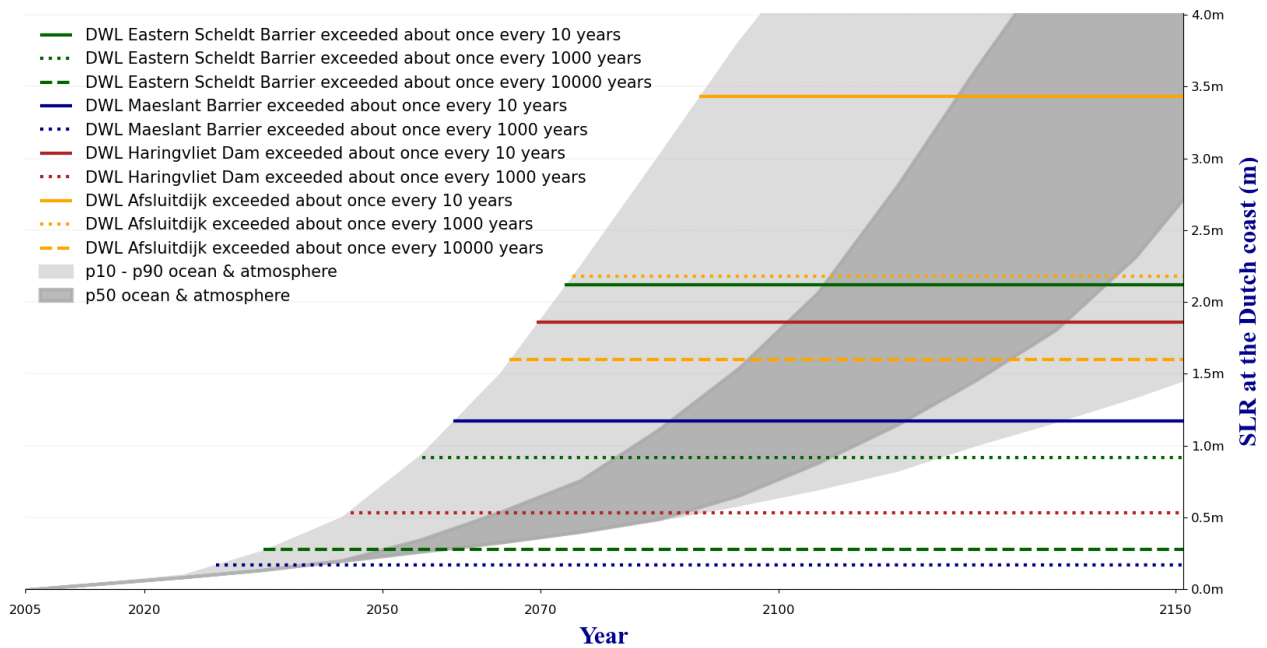


Figure 14: SLR at the Dutch coast w.r.t. 1995-2014 following the successive collapse of different Antarctic basins under a SSP585-forcing scenario. Horizontal lines indicate how SLR impacts the exceedence probability of the design water levels of the Eastern Scheldt Barrier, Maeslant Barrier, Haringvliet Dam and Afsluitdijk. In grey the maximum p10-p90 uncertainty range for the combined oceanic and atmospheric collapse criteria. In darkgrey the p50 for the combined ocean & atmosphere.

Figure 14 shows the exceedence probability of the design water levels of the Eastern Scheldt Barrier, Maeslant Barrier, Haringvliet Dam and Afsluitdijk. These barriers are designed to withstand floods that are statistically unlikely to occur more than once in 1000-100,000 years.

However, as sea levels rise the design water levels of the Barriers will be exceeded more frequent. As the envisioned lifetime of these structures is typically 100-200 years (Haasnoot et al., 2020), SLR has the potential to significantly reduce the functional lifetime of the Barriers when the flood safety standards are no longer met. For some of these defence structures, a rising sea level will more and more hamper the gravity draining of excess water, so that structural pumping is needed to discharge the water. For the Afsluitdijk structural pumping is needed beyond 0.65m of SLR, which can happen as soon as 2047 in the worst case SLR scenario.

To illustrate the "usage" of Figures 13 and 14, we discuss a scenario wherein the Eastern Scheldt Barrier needs to be replaced when it has to be closed for more than 10x per year. Depending on the SLR scenario that we use, the point in time where the barrier fails to meet this standard is ~ 2050 at the earliest, ~ 2100 at the latest and ~ 2080 ('69-'94) for the median percentile of the ensemble. Assuming ~ 30 years for planning and implementation (Haasnoot et al., 2020), a decision on the reinforcement of the Eastern Scheldt Barrier would have to be taken anywhere between now and the next 50 years (17-42 years for the p50). This example highlights the deep uncertainty that is surrounding the high-end SLR projections from Antarctica and emphasizes the strong need to better curtail these projections. Higher closing criteria will delay the timing of the adaptation tipping point but would have to go with reinforcements of the upstream river dikes or a higher risk acceptance (Section 4.6).

Also, preparatory actions can reduce the time that is needed for design and implementation ("lead time"), so that high-impact decisions can be taken at a later moment in time when there is (hopefully) less uncertainty.

A long-term perspective can help to overcome decision paralysis on the short- and mid-term. By 2090 the p90 of the SLR projection range forecasts a SLR of ~ 3.5 m, a value that is reached by 2200 for the p10 of the ensemble. The lower bound and upper bound of the combined p50 range reach the 3.5m at ~ 2160 and ~ 2120 , respectively (Figure S5). Even though the uncertainty in the p50 is about 40 years, it seems justifiable to anticipate a longterm SLR of 3.5m. Recall that the envisioned lifetime of the larger defence structures is on the order of 100-200 years (Table 1, Haasnoot et al., 2020). In the more "positive" warming scenarios that include Antarctic ice shelf collapse, this functional lifetime can still be realised. In the more pessimistic case, raising the safety standards of the original structures provide a better starting point for follow-up measures. Flexible measures with a short lead- and lifetime can complement this strategy but are inferior to the larger measures when taking on a longterm perspective.

Either way, monitoring and detecting early warning signals for rapid SLR will be essential in the coming decades. Ideally, these signals have discriminatory value i.e. they make it unlikely or rule out certain possibilities for the future evolution of the sea level. The strength of the signpost is also determined by the time difference between the emergence of the signpost and the timing of the adaptation tipping point. The longer this time stretch is, the more

time there is to overthink alternative and/or complementary strategies that also consider low-regret options. This reduces the risk of taking unnecessary high-impact decisions.

Using the data from this study, it is not possible to identify reliable/robust signposts that discriminate between the different SLR scenarios, because the methodological uncertainties and the uncertainties in the projected basal melt are so large. Figures 9 and S2 indicate that the spatial patterns of mass loss are largely similar - i.e. when ice is lost, it is often drained from the same regions but the timing may differ - so that these patterns have little discriminatory value in itself. The timing of basin collapse could be a promising discriminatory signpost, but is poorly constrained because of the large intermodel spread in the projected basal melt. The uncertainty in the timing of collapse is carried over to the SLR projections, so that the magnitude and rate of SLR are also poorly constrained and lose their discriminatory power.

4 Discussion

4.1 Considerations for the basal melt

In this section we want to reflect on the sub-shelf melting protocol of the ISMIP6, and the veracity of the realized basal melt dataset. In this regard, we want to address two topics:

1. Our reservations on the horizontal extrapolation of the open ocean water properties into the (larger) ice shelf cavities.
2. Our thoughts on the applicability of the PIGL and MeanAnt calibrations for the whole of Antarctica, and a recommendation to improve this calibration.

We conclude with talking about the possible implications of using shelf-averaged melt rates rather than the melt rates at the GL (Section 2.1.4) to estimate the thickness change of the ice shelves.

As mentioned in Section 2.1.2, Jourdain et al. (2020) horizontally extrapolate the open ocean water properties from the observed climatology and CMIP5 into the ice shelf cavities. Whereas the exchange with the open ocean may be considerable for the smaller ice shelf cavities like Pine Island Glacier and Thwaites Glacier, the assumption that vertical and horizontal ocean properties are retained in the larger ice shelf cavities is doubtful. Water masses in e.g., the larger cavities of the Ross and Filchner-Ronne ice shelves, are typically below the surface freezing point as a result of the high pressure and entrainment of meltwater (Silvano et al., 2016). Indeed, the GL from these larger "cold cavity" ice shelves may not be subjected to the open ocean conditions when the sustained circulation in the cavity is small and the cavity entrance is tens of kilometers away (Reese et al., 2018). Horizontal extrapolation of the open ocean water properties underneath the larger ice shelves may thus result in an overestimation of the thermal forcing at the GL of these typically large cold cavities, and by extension of the modelled basal melt.

Our second comment is on the tuning of the basal melt parameterization. As mentioned in Section 2.1.2, this parameterization is dependent on two coefficients that are tuned to the observations by means of a two-stage calibration procedure. The γ -coefficient determines the sensitivity of the parameterization to an increase in the thermal forcing, and is calibrated first. The γ -coefficient is kept constant for all of Antarctica and is calibrated to reproduce the mean Antarctic melt rate (MeanAnt) or the highest melt rates near the deep GL of Pine Island Glacier (PIGL). Next, thermal forcing corrections are applied to reproduce the patterns of observed mass loss at the scale of the individual drainage basins (Jourdain et al., 2020). Because of the use of a single, Antarctica-wide γ -coefficient, the MeanAnt calibration tends to underestimate the melt rates in the Admundsen sector. On the contrary, the PIGL method reproduces the high melt near Pine Island but overestimates melt rates in almost all other cavities (Jourdain et al., 2020). It seems that the MeanAnt calibration is unable to capture the melt rates in the small and warm cavities, whereas the PIGL calibration is too melt-sensitive to adequately reproduce the basal melt rates in the (larger) cold cavities. Indeed, as the majority of the ice shelf cavities around Antarctica are "cold", using PIGL for the entire continent is arguably unrealistic (Figure 15). Looking at Figure 15, one might argue that a combination of the two γ -coefficients, namely γ -PIGL for region A and γ -MeanAnt for region B, would yield more realistic basal melt sensitivities Antarctica-wide. As a result, the total spread in the basal melt might be significantly reduced, and with that also the spread in the SLR projections (Figures 8 & 12).

In Section 2.1.4 we mentioned that we use shelf-averaged melt rates rather than e.g., melt rates at the GL, for our analysis. Of course, this has implications for the ocean-induced thickness change that we calculate, and therefore also for the exceedence time of the damaged and critical ice thickness thresholds (Section 2.2.2). Observational data products tend to show a typical pattern of comparably high melting near the GL and lower melting or refreezing towards the calving front, and this pattern was also reproduced by Jourdain et al. (2020). Importantly, the high melt rates near the deep grounding lines of the ice shelves are thought to act as the primary control on the observed increases in ice discharge from glaciers in the Bellinghausen and Amundsen Sea Sectors (e.g. Pritchard et al. 2012; Reese et al. 2018). In a next study it would therefore be interesting to compare the effects of using both shelf-averaged melt rates and GL melt rates for the results of our analysis. We anticipate that the usage of GL melt rates results in a higher SLR by 2100 (2200) than the usage of shelf-averaged melt rates.

4.2 Rationale for the separate treatment of the ice-dynamic modelling and the stability analysis

In this study, the stability analysis of the ice shelves and the ice-dynamic modelling are performed independent of each other. Although we do believe that an integration of the two would constitute the best way forward (Section 4.7), we did not do this in this study for two reasons:

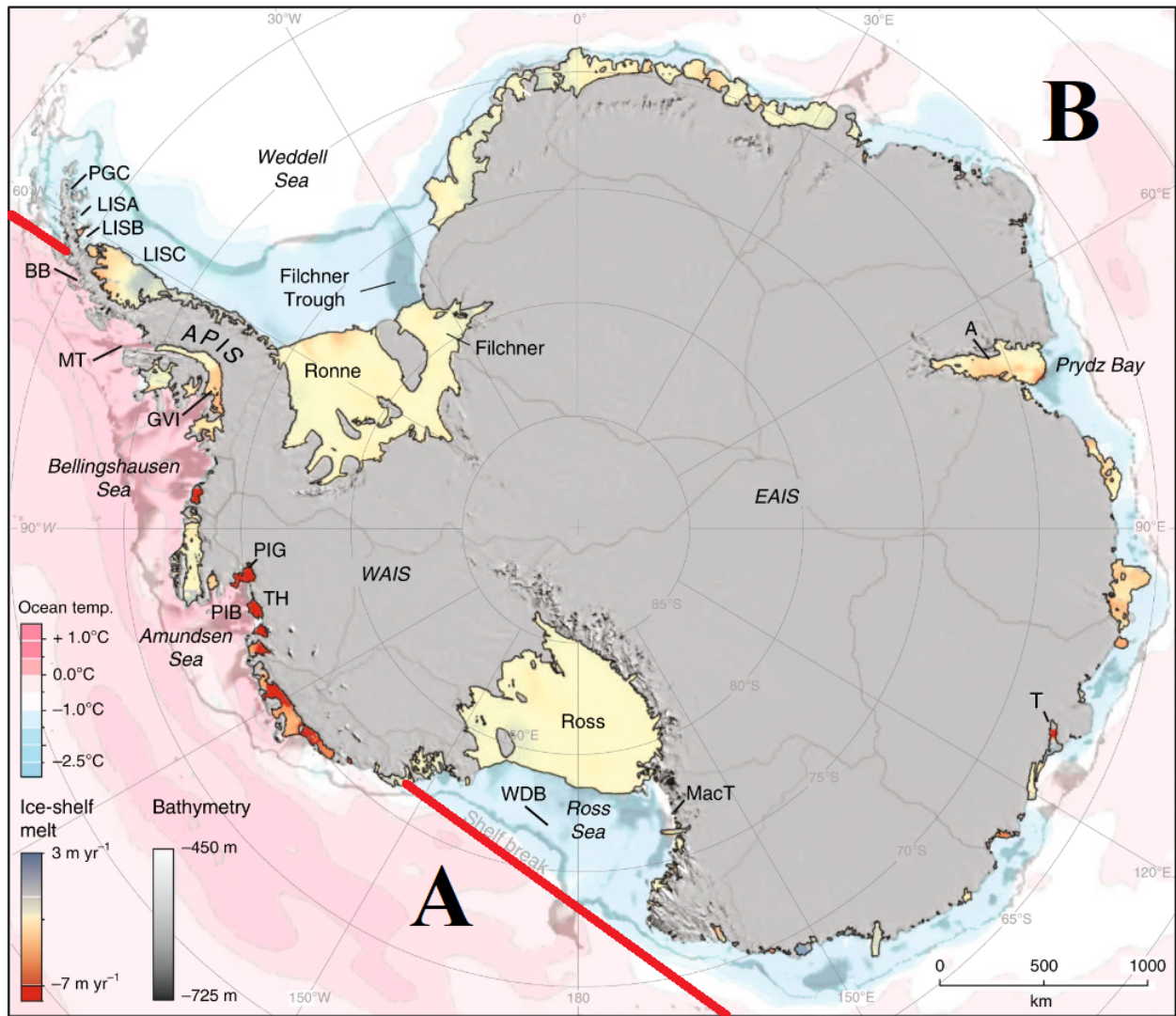


Figure 15: Adapted Figure from Smith et al. (2019) showing the rate of ice thickness change of the Antarctic ice-shelves. Also shown is the estimated average seafloor potential temperatures in °C from the World Ocean Atlas. Generally speaking, ice shelf cavities to the left of the red line (region A) are *warm*, whereas the ice shelf cavities in region B are *cold*.

1. Adequately solving for the ice/ocean/atmosphere-interactions at model runtime requires a higher model resolution and/or better parameterizations of the physics involved than is currently supported by IMAU-ICE. Improvements are especially warranted when it comes to (the sub-grid parameterization of) the sub-shelf melting in the model. The developers of the IMAU-ICE model have already announced a complete overhaul of the current sub-shelf melting scheme in the model (Berends et al., 2022), but this would otherwise also have been beyond the scope of this study.

2. By decoupling the stability analysis and the ice-dynamic modelling, we might just as well assume an equilibrium ice sheet and present-day forcings. This allows for simplifications that reduce the uncertainty from the model numerics and model physics, and relaxes the model resolution requirements: If the modelled ice sheet is in steady-state, this means that the surface mass balance and basal mass balance are close to neutral and the GL position is more or less fixed. Prescribing a near zero basal mass balance is akin to saying the ocean-induced sub-shelf melting is nihil, so that we can factor out this part of the model and with that the uncertainties from the choice for a sub-grid melting scheme (Leguy et al. 2021, Section 4.3).

We hope that differences between model runs are then principally caused by prescribed differences in the timing of collapse of the different basins, and not by the model physics and numerics. Indeed, we assume that the uncertainty arising from the forcing of the ice shelf collapse is larger than the uncertainty arising from the ice dynamics itself.

There are a few more points that we want to address:

- We make the assumption that the buttressing capacity of the ice shelves is not significantly reduced until the moment of collapse, so that the GL flux and related GL position don't change much up to this point. We have to make this assumption, because the GL dynamics are not included in the stability analysis if we do not interactively model the ice dynamics. GL motion has the potential to significantly delay (advance) the moment of collapse when the GL retreats to a place that is less (more) exposed to the warmer ocean waters. This is unfortunately not a very strong assumption: a reduction in buttressing has already caused a measurable retreat of the GL from e.g., Pine Island Glacier, Thwaites Glacier and Totten Glacier, as well as a speedup of their tributary glaciers (e.g., Christie et al., 2016; Rignot et al., 2014; Konrad et al., 2018).
- It is possible that the collapse of an ice shelf has a destabilizing effect on its neighbouring ice shelves, or even triggers their collapse. However, because the ice shelf stability analysis is not integrated with the ice-dynamic model, we cannot have such a cascading effect in the stability analysis at front. In the ice-dynamic modelling part this is no longer the case, and in practise we see that especially the collapse of one of the basins in the WAIS region does not leave the other basins unaffected (e.g. Figure 9).

4.3 Sensitivity to the model resolution

Berends et al. (2022) have repeated the ABUMIP-experiment at resolutions of 40, 32, 20, and 16km in their benchmark paper for the IMAU-ICE model. They concluded that the model resolution has a negligible effect on the results from the ABUK-experiment. However, the same is not always true for the ABUM-experiment that prescribes an extreme sub-shelf melt rate. The latter is dependent on the choice for a sub-grid parameterization of the sub-shelf melting that can have a strong effect on the modelled GL flux (Leguy et al.,

2021). IMAU-ICE implements three sub-grid parameterizations, namely no melt or full melt depending on a flotation criterion (FCMP), melt scaled with the sub-grid floating fraction (PMP), and a parameterization that only applies melt to fully floating grid cells (NMP). Preliminary results from Berends et al. (2022) showed that the end-member SLR from the ABUM-experiment could differ by as much as a factor 2 from the choice of one of these sub-grid schemes alone. More so, they found that the modelled SLR from the NMP and PMP parameterizations depended considerably on the grid resolution. Considering all this, we finally decided to use the ABUK-approach for our analysis. Not only does its usage relax the resolution requirements of the ice model, it has the additional benefit that its model implementation is more straightforward.

4.4 Sensitivity to the subglacial hydrology and basal mechanics

Subglacial hydrology and basal mechanics constitute a major uncertainty in both the modelling of marine ice sheets and in our physical understanding. The sliding of ice is dependent on multiple factors such as the rheologic conditions at the ice sheet base (temperature & viscosity) and the bed roughness. These factors determine the effective pressure, deformation type and sliding rate at the rock-ice interface (e.g., Gladstone et al., 2017; Joughin et al., 2019), and therefore play a decisive role in regulating the ice flux across the GL.

A variety of sliding/friction laws are in use between the different ice sheet models. Indeed, several studies have related the substantial uncertainties in the projected ice-sheet retreat to the considerable uncertainty that remains in the treatment of the basal roughness, friction, and sliding (Sun et al., 2020; Pattyn et al., 2017).

4.5 Comparison to other studies

To the best of our knowledge, this is the first study that performed an ice shelf instability analysis at the continental scale and used this information to simulate the Antarctic mass loss from a reduced buttressing over time. Nonetheless, there is some overlap with the ABUMIP-experiment from Sun et al. (2020). Recall that ABUMIP-experiment was designed to investigate how changing ice shelves control Antarctic mass loss independent of the triggers for how and when ice shelves weaken. This experiment allowed them to give an estimate of the uncertainty that is caused by the variation between the ice sheet models. Our results complement those from the ABUMIP-experiment because we now also have an uncertainty estimate from the triggers of ice shelf collapse.

ABUMIP-ABUK gives a large uncertainty range for the future sea level: the participating models predicted a SLR anywhere between 1-8m (1-10m) over 200 (500) years from now. (IMAU-ICE is at the high-end of this projection range but recent (and not yet published) developments in the initialization of the model have already significantly lowered the SLR estimates from this model). Our trigger-based uncertainty estimate gives a maximum SLR

spread of $\sim 0\text{-}3\text{m}$ by 2100, and $\sim 1.6\text{-}6\text{m}$ by 2200. This means that the uncertainty caused by the variation between the ice sheet models is about 2.3x as large as the uncertainty caused by the triggers of ice shelf collapse, namely 3m (4m) versus 7m (9m) by 2100 (2200). If the main goal is to reduce the SLR uncertainty from a large dynamic contribution of the AIS, curbing - or at least attributing - variations between ice sheet models seems more urgent/promising than the development of better predictions for the sub-shelf melting.

Unlike Sun et al. (2020), this study is not a model intercomparison effort because we only accessed one ice sheet model. However, since the thresholds for instability are evaluated independent of IMAU-ICE, the experiment can easily be extended to the other models participating in the ISMIP6-effort. Indeed, the timeline-based approach developed for this study can help with the design of a new model intercomparison project that investigates both intermodel differences and the triggers and thresholds for ice shelf collapse.

4.6 Considerations for the timing of adaptation tipping points

So far, we have only considered the feasibility of hard- and soft-engineering options for flood defence in our analysis on the timing of adaptation tipping points. However, the timing of an adaptation tipping point is also strongly influenced by our acceptance of risk. If we "accept" more frequent flooding or a higher probability of failure, the timing of an adaptation tipping point shifts backwards. In this view, the timing of adaptation is also dependent on socioeconomic factors and political deliberations. Indeed, socioeconomic considerations have already led to a considerable spatial differentiation in the levels of accepted flood risk in the Netherlands (van Rijswijk et al., 2015).

From a socioeconomic perspective, it is also possible to relax the flood risk standards of our defence works without accepting a higher level of risk for the collective. Public-private flood insurance schemes for ex-post compensation of flood damage form a good example, because the extra socioeconomic risk from a lowering of the flood defence standards can be spread amongst many. These schemes may at the same time increase the public awareness over flood risks (Surminski et al., 2015). Such a diversification of flood risk management strategies is good for building flood resilience and has the ability to relax the design standards of the flood defence works without increasing the total socioeconomic costs of a flooding event.

4.7 Outlook

Ideally, the stability analysis and the ice-dynamic modelling will be integrated in a future study. This allows for feedbacks between the oceanic & atmospheric forcings and the ice sheet that have the potential to significantly increase the veracity of the projections. To achieve this in IMAU-ICE, the first part that needs to be revisited is the basal melt module. The current model version supports a (linear) temperature/depth-dependent sub-shelf melt parameterization by Martin et al. (2011), and an option for prescribing a spatially uniform

sub-shelf melt rate. However, in recent years new and more complex basal melt parameterizations that are also able to capture the effect of the ocean circulation underneath the ice shelf (e.g. Lazeroms et al., 2019; Reese et al., 2018), have been developed. IMAU-ICE should now implement several of these newer parameterizations and evaluate their performance regarding the modelling of the GL dynamics and the ability to reproduce the observed patterns of basal melt underneath the ice shelves. There should also be the option to prescribe oceanic temperature and salinity fields from the CMIP5/6 to facilitate model intercomparison efforts. Also, the initialization procedure of the model needs to be improved. An initialization of IMAU-ICE that captures both the present-day ice sheet geometry and is in steady state is not yet realized and this can have significant impact on (the interpretation of) the results. For instance, in the ABUMIP-experiments the control was not subtracted from the model results even though there was still a 1m (multi-meter) GMSLR in the control run from IMAU-ICE over a 200 (500) year model period (Figure S6). As mentioned in Section 2.3.2 this may be attributed to a deep uncertainty surrounding the correct tuning of such parameters as the rheology of the ice and the basal friction at the ice-bedrock interface, caused by a lack of observations. Also, there is a lack of observations on the actual melt rates at the ice shelf bases. As these issues will probably not be resolved anytime soon, the IMAU-ICE modelling group is now looking into promising inverse modelling techniques to find the "right" basal sliding coefficients, ice conditions and basal melt to achieve a steady-state at the present-day ice geometry. The reader is pointed at Bernales et al. (2017) for more information on such techniques.

5 Conclusion

In this study we researched the dynamic SLR contribution from Antarctic ice shelf collapse, and its implications for adaptive planning in the Netherlands. We first performed a stability analysis to find out when the Antarctic ice shelves could become conditionally unstable under the influence of the atmosphere, ocean, or a combination of the two. On the condition of instability, we modelled the collapse of the ice shelves in an ice-dynamic model and calculated the resultant sea level rise. By repeating this process for different stability criteria we can get an uncertainty estimate for both the triggers of Antarctic ice shelf collapse and the consequent GMSLR. The GMSLR projections were then translated to a SLR uncertainty range at the Dutch coast, and compared to the design water levels and intended closing frequencies of the major storm surge barriers. By augmenting the result from this analysis with the time that is needed to plan and implement for a reinforcement of the barriers, we obtained an estimate for the last possible moments in time when a decision on an adaptive measure may be taken.

We conclude that both the magnitude and the timing of larger scale SLR from Antarctic ice shelf collapse is principally controlled by the ocean-induced thinning. Notwithstanding, atmospheric forcings have the ability to slightly expedite the moment of collapse leading to a marginally higher SLR after the 200 year study period. We further assess that larger scale

ice shelf collapse is unlikely before the early second half of the 21st century, and that the resultant dynamic SLR will become important in the mid- to late second half of this same century.

In all but the lowest basal melt scenarios we find that the West Antarctic Ice Sheet is (almost) completely lost by 2200, causing a GMSLR totalling 0.07-0.68m by 2100, and 2.5-3.2m by 2200. The contribution from the Antarctic Peninsula is only marginal, but the combined East and North Antarctic Ice Sheet add an additional 1-2m to the final projections (median estimates for the basal melt). However, the GMSLR can still be considerably less (more) when using lower (higher) estimates for the basal melt.

When comparing our results to Sun et al. (2020), we find that the uncertainty caused by the variation between the ice sheet models is about 2.3x larger than the uncertainty caused by the triggers for ice shelf collapse. These findings suggest that if we want to better curtail the SLR uncertainty from a large dynamic contribution of the Antarctic Ice Sheet, curbing - or at least attributing - variations between ice sheet models is more important than the development of better predictions for the sub-shelf melting.

Reducing the uncertainty in the basal melt is again key if we wish to identify reliable and discriminatory signposts for a large dynamic contribution from Antarctica. Despite the large uncertainties in our analysis, we have reasons to believe that the timing, rate and magnitude of SLR have more discriminatory power than the spatial patterns of mass loss. That is, because mass loss often occurs in the same regions but the timing of collapse may differ considerably.

We agree with Haasnoot et al. (2020) that a long-term perspective on SLR can help policy makers to overcome decision paralysis on the short- to mid-term. Indeed, when Antarctic ice shelf collapse becomes a distinct possibility, it is likely not a matter of *if* and *how* to adapt to certain levels of SLR, but *when* to adapt. Flexible measures with a short lead- and lifetime can play a role in the adaptive strategy, but are inferior to larger measures for an extreme sea level rise scenario like the one considered here, or when taking on a long-term perspective.

6 Supplementary Material

SLR wrt 1995-2014 following the collapse of different Antarctic basins using only atmospheric constraints

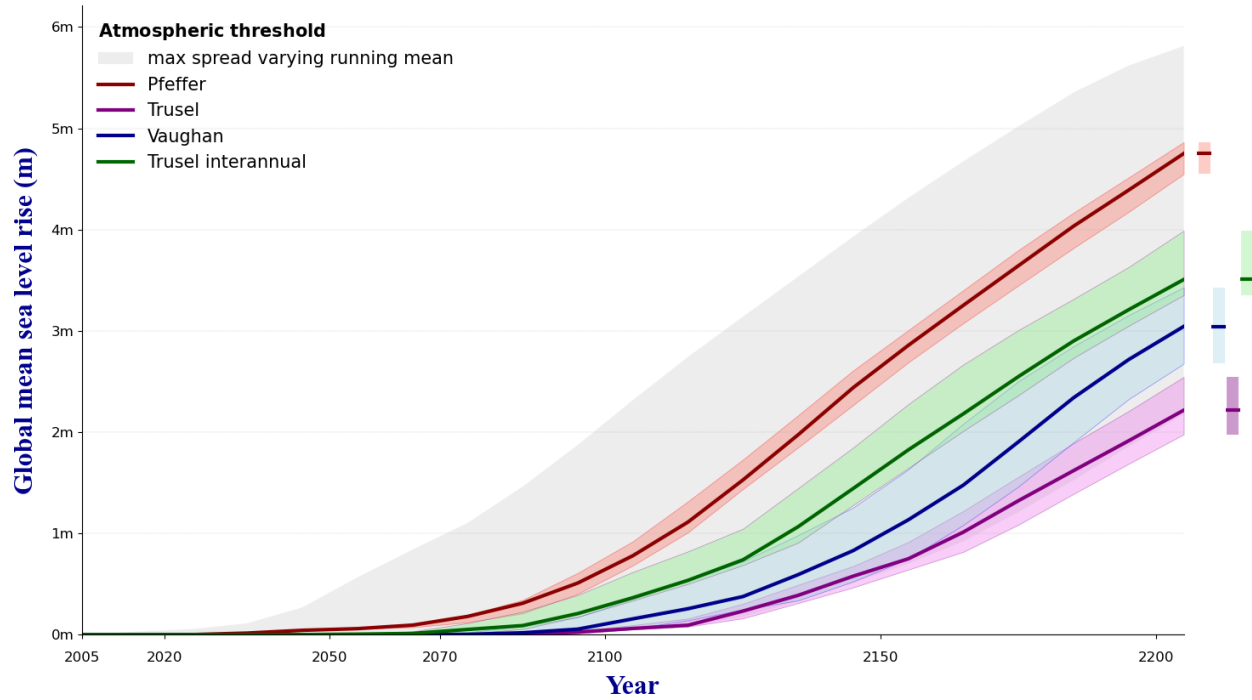
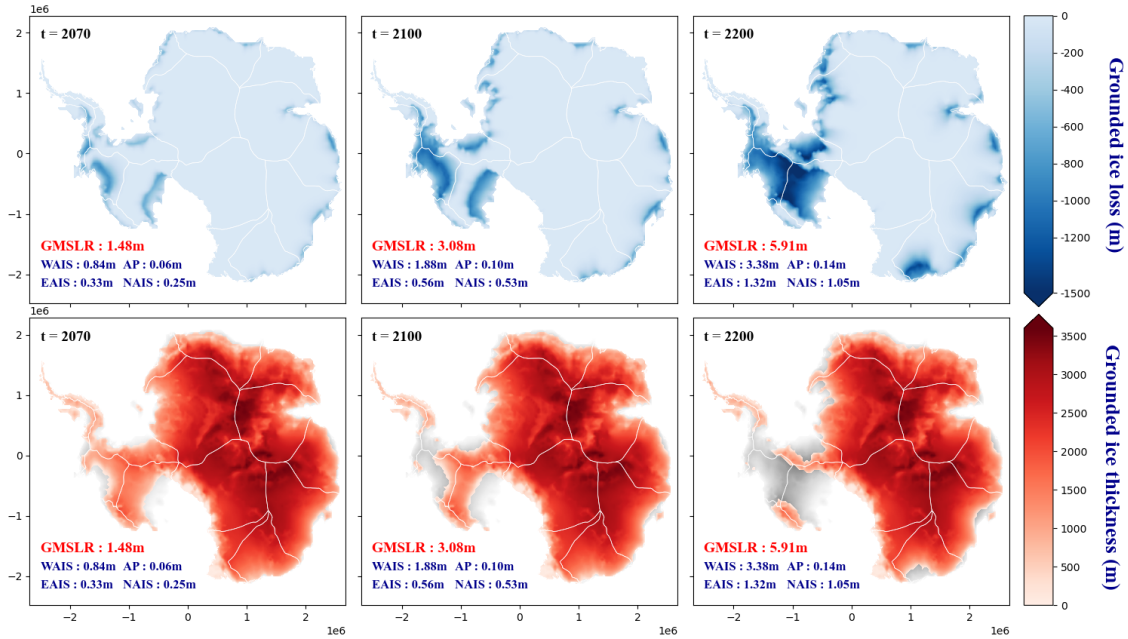


Figure S1: GMSLR w.r.t. 1995-2014 following the successive collapse of different Antarctic basins under a SSP585-forcing pathway using only atmospheric criteria for estimating the timing of collapse. The SLR uncertainty bandwidth for the Trusel criterion (purple) was obtained by varying the threshold for conditional instability between 650 and 800 mm w.e. yr^{-1} . Likewise the Pfeffer criterion (red) was varied between 0.6 and 0.8, Vaughan (blue) between -10 and -8°C , and Trusel interannual (green) between 650 and 800 mm w.e. yr^{-1} . Solid lines show the SLR resulting from the mid-values in these ranges. We used a 5-year running mean for the Vaughan and Pfeffer criteria and a 10-year running mean for the Trusel criterion. For Trusel interannual the criterion had to be exceeded 3x in a period of 5 years. In lightgrey, the total SLR projection bandwidth that follows from using a 1-year (upper bound) and 30-yr running mean (lower bound). See also Figure S3.

Grounded ice thickness change (m) wrt 1995-2014 under SSP85 using Pfeffer and the PIGL calibration



Grounded ice thickness change (m) wrt 1995-2014 under SSP85 using Trusel and the MeanAnt calibration

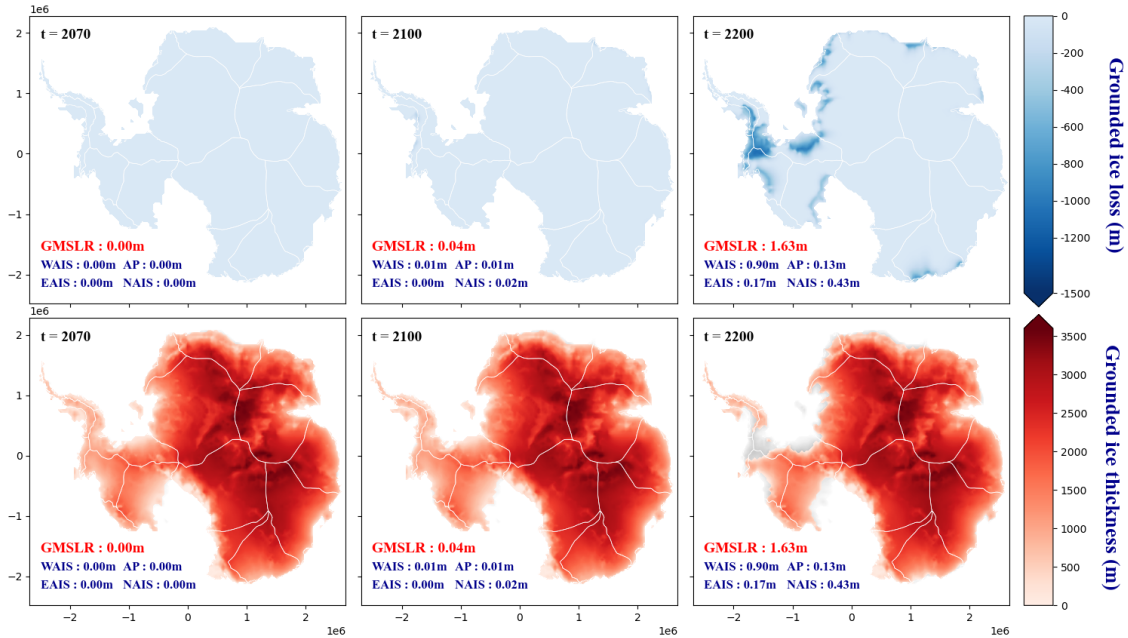


Figure S2: Loss of ice mass above flotation (blue panels) and the absolute thickness change (red panels) for the orange dotted lines in Figure 8. Top two panel rows use the 90th percentile of the basal melt ensemble, and the most pessimistic ocean & atmosphere threshold/calibration combination (Pfeffer 0.6, PIGL). Bottom panel rows use the 10th basal melt percentile and the most conservative ocean & atmosphere threshold/calibration combination (Trusel 650, MeanAnt). WAIS: basin 3 & 7-11; EAIS: basin 13-15, AP: basin 4-6, NAIS: basin 1,2 & 16-18.

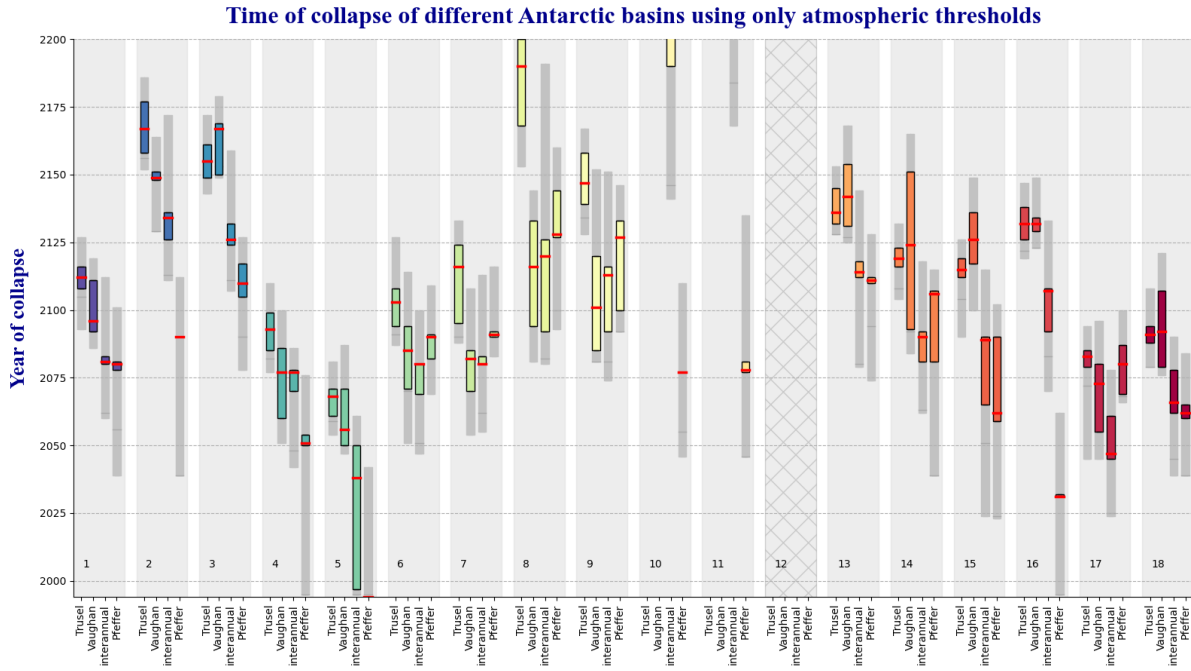


Figure S3: Time of collapse of the different Antarctic basins under SSP585 using only atmospheric constraints. Shown for each basin is the uncertainty in the timing of collapse. In color the uncertainty bandwidth obtained by varying the Trusel (interannual) threshold criterion between 650 and 800 mm w.e. yr⁻¹ after applying a 10 (5)-year running mean filter to the time series. Likewise the Pfeffer criterion was varied between 0.6 and 0.8 and the Vaughan criterion between -10 and -8°C, again after applying a 5-year running mean filter to the time series. The grey uncertainty bar was obtained by varying the running mean between 1 and 30 years. Basins 12 is excluded from the analysis and not featured here.

Basin	MeanAnt			MeanAnt + S			PIGL			PIGL + S		
	90th	50th	10th	90th	50th	10th	90th	50th	10th	90th	50th	10th
1	-5	2139	+16	-13	2145	+7	-69	2121	>79	-25	2143	+18
2	-29	2154	+17	-17	2159	+10	-41	2109	>91	-37	2152	+20
3	-20	2142	+17	-13	2149	+8	-41	2104	>96	-30	2144	+15
5	-12	2072	+6	-14	2074	+5	-31	2068	+22	-24	2074	+8
6	-113	2113	+5	-114	2114	+4	-114	2114	+7	-115	2115	+6
7	-53	2117	>83	-54	2130	+19	-38	2057	>143	-71	2109	+35
8	-33	2093	+91	-29	2083	+32	-23	2048	+52	-22	2061	+44
9	-35	2142	>58	-29	2121	+18	-30	2072	>128	-34	2095	+30
10	-28	2132	+60	-36	2174	+22	-47	2094	+64	-39	2145	+35
11	-41	2134	>66	NC	NC	NC	-50	2087	>113	-61	2153	>47
13	-18	2116	+23	-26	2105	+28	-25	2080	>120	-27	2092	+41
14	NC	NC	NC	-24	2083	>117	-32	2075	>125	-19	2066	+43
15	-35	2085	>115	-19	2074	>126	-19	2044	+41	-15	2057	>143
16	NC	NC	NC	NC	NC	NC	-21	2075	+47	-15	2094	>106
18	-19	2111	+5	-15	2112	+3	-39	2093	+27	-27	2108	+7

Figure S4: Uncertainty in the timing of collapse (years) of the different Antarctic basins using different percentiles for the basal melt and no atmospheric constraints. Data are based on the data in Figure 11. Numbers in the p90 and p10 columns are relative to the collapse year in the p50 column. E.g., using the MeanAnt calibration, basin 1 collapses in 2139 for the p50, 2134 for the p90 and 2155 for the p10. When a basin collapses for the p50 of the model ensemble but not for the p10, a ">"-sign is introduced to provide some estimate for the uncertainty in the timing of collapse. "NC" indicates that the basin does not collapse at all. Basins 12 is excluded from the analysis and not featured here. The ice shelves in basin 4 and 17 are already thinner than 200m from the start and are also excluded.

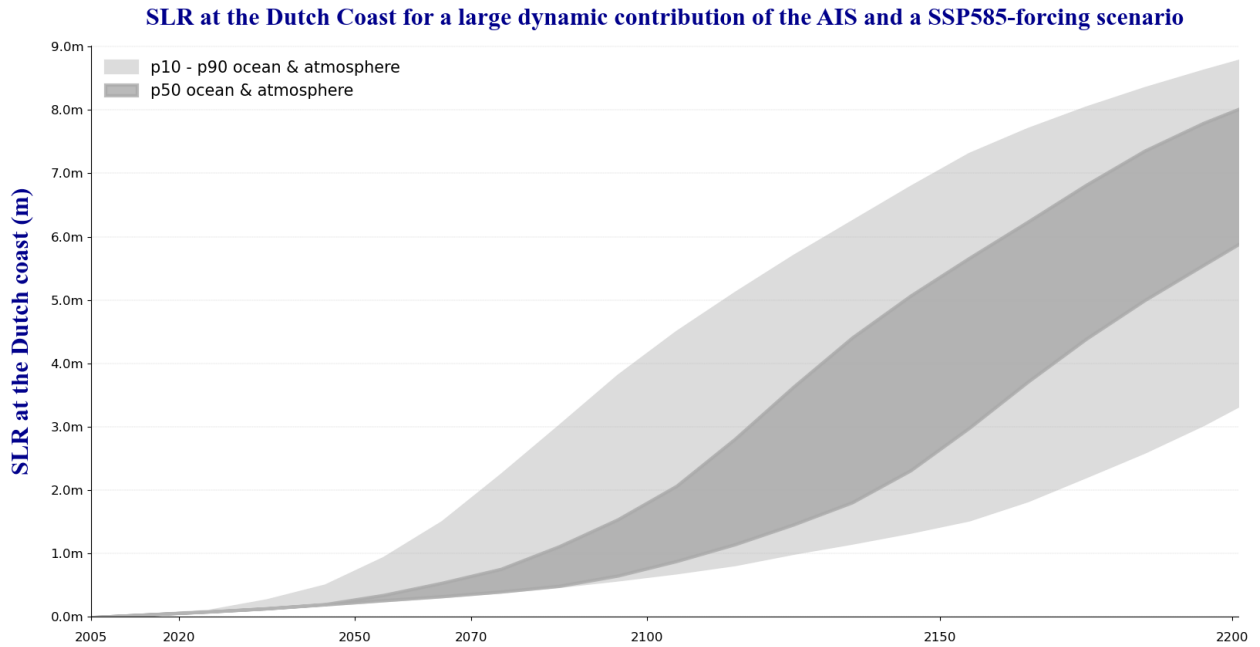


Figure S5: SLR at the Dutch coast w.r.t. 1995-2014 following the successive collapse of different Antarctic basins under a SSP585-forcing scenario. In grey the maximum p10-p90 uncertainty range for the combined oceanic and atmospheric collapse criteria. In darkgrey the p50 for the combined ocean & atmosphere.

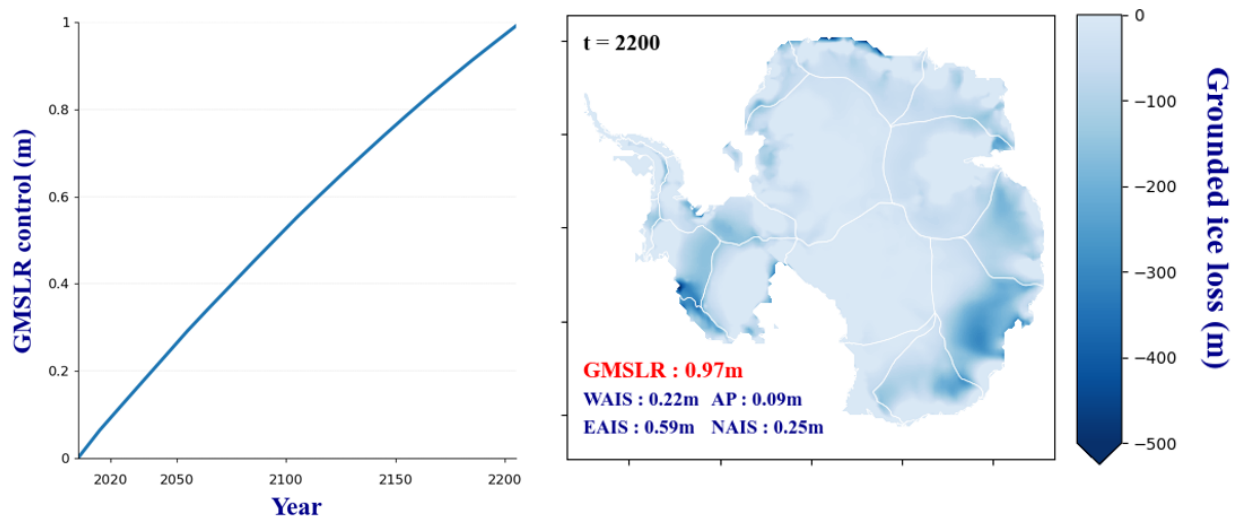


Figure S6: GMSLR w.r.t. 1995-2014 in the control run.

References

- Bassis, J. N., & Walker, C. C. (2012). Upper and lower limits on the stability of calving glaciers from the yield strength envelope of ice. *Proceedings of the Royal Society A: Mathematical, Physical and Engineering Sciences*, *468*(2140), 913–931.
- Bell, R. E., Banwell, A. F., Trusel, L. D., & Kingslake, J. (2018). Antarctic surface hydrology and impacts on ice-sheet mass balance. *Nature Climate Change*, *8*(12), 1044–1052.
- Berends, C. J., Goelzer, H., Reerink, T. J., Stap, L. B., & van de Wal, R. S. (2022). Benchmarking the vertically integrated ice-sheet model imau-ice (version 2.0). *Geoscientific Model Development Discussions*, 1–28.
- Berends, C. J., Goelzer, H., & Van De Wal, R. S. (2021). The utrecht finite volume ice-sheet model: Ufemism (version 1.0). *Geoscientific Model Development*, *14*(5), 2443–2470.
- Bernales, J., Rogozhina, I., & Thomas, M. (2017). Melting and freezing under antarctic ice shelves from a combination of ice-sheet modelling and observations. *Journal of Glaciology*, *63*(240), 731–744.
- Burgard, C., Jourdain, N. C., Reese, R., Jenkins, A., & Mathiot, P. (2022). An assessment of basal melt parameterisations for antarctic ice shelves. *The Cryosphere Discussions*, 1–56.
- Christie, F. D., Bingham, R. G., Gourmelen, N., Tett, S. F., & Muto, A. (2016). Four-decade record of pervasive grounding line retreat along the bellingshausen margin of west antarctica. *Geophysical Research Letters*, *43*(11), 5741–5749.
- Favier, L., Jourdain, N. C., Jenkins, A., Merino, N., Durand, G., Gagliardini, O., . . . Mathiot, P. (2019). Assessment of sub-shelf melting parameterisations using the ocean–ice-sheet coupled model nemo (v3. 6)–elmer/ice (v8. 3). *Geoscientific Model Development*, *12*(6), 2255–2283.
- Feldmann, J., Albrecht, T., Khroulev, C., Pattyn, F., & Levermann, A. (2014). Resolution-dependent performance of grounding line motion in a shallow model compared with a full-stokes model according to the mismip3d intercomparison. *Journal of Glaciology*, *60*(220), 353–360.
- Fox-Kemper, B., Hewitt, H. T., Xiao, C., Aalgeirsdóttir, G., Drijfhout, S. S., Edwards, T. L., . . . Yu, Y. (2021). IPCC AR6 WG1, chs. 9: Ocean, cryosphere and sea level change. Cambridge University Press. In Press.
- Fretwell, P., Pritchard, H. D., Vaughan, D. G., Bamber, J. L., Barrand, N. E., Bell, R., . . . others (2013). Bedmap2: improved ice bed, surface and thickness datasets for antarctica. *The Cryosphere*, *7*(1), 375–393.

- Gladstone, R. M., Warner, R. C., Galton-Fenzi, B. K., Gagliardini, O., Zwinger, T., & Greve, R. (2017). Marine ice sheet model performance depends on basal sliding physics and sub-shelf melting. *The Cryosphere*, *11*(1), 319–329.
- Goldberg, D. N. (2011). A variationally derived, depth-integrated approximation to a higher-order glaciological flow model. *Journal of Glaciology*, *57*(201), 157–170.
- Gudmundsson, G. H., Paolo, F. S., Adusumilli, S., & Fricker, H. A. (2019). Instantaneous antarctic ice sheet mass loss driven by thinning ice shelves. *Geophysical Research Letters*, *46*(23), 13903–13909.
- Haasnoot, M., Kwadijk, J., Van Alphen, J., Le Bars, D., Van Den Hurk, B., Diermanse, F., . . . Mens, M. (2020). Adaptation to uncertain sea-level rise; how uncertainty in antarctic mass-loss impacts the coastal adaptation strategy of the netherlands. *Environmental research letters*, *15*(3), 034007.
- Hay, C., Mitrovica, J. X., Gomez, N., Creveling, J. R., Austermann, J., & Kopp, R. E. (2014). The sea-level fingerprints of ice-sheet collapse during interglacial periods. *Quaternary Science Reviews*, *87*, 60–69.
- Huybrechts, P. (1992). *The antarctic ice sheet and environmental change: a three-dimensional modelling study* (Unpublished doctoral dissertation). Vrije Universiteit of Brussel.
- Jenkins, A., Shoosmith, D., Dutrieux, P., Jacobs, S., Kim, T. W., Lee, S. H., . . . Stammerjohn, S. (2018). West antarctic ice sheet retreat in the amundsen sea driven by decadal oceanic variability. *Nature Geoscience*, *11*(10), 733–738.
- Joughin, I., Smith, B. E., & Schoof, C. G. (2019). Regularized coulomb friction laws for ice sheet sliding: Application to pine island glacier, antarctica. *Geophysical research letters*, *46*(9), 4764–4771.
- Jourdain, N. C., Asay-Davis, X., Hattermann, T., Straneo, F., Seroussi, H., Little, C. M., & Nowicki, S. (2020). A protocol for calculating basal melt rates in the ismip6 antarctic ice sheet projections. *The Cryosphere*, *14*(9), 3111–3134.
- Kittel, C., Amory, C., Agosta, C., Jourdain, N. C., Hofer, S., Delhasse, A., . . . others (2021). Diverging future surface mass balance between the antarctic ice shelves and grounded ice sheet. *The Cryosphere*, *15*(3), 1215–1236.
- Konrad, H., Shepherd, A., Gilbert, L., Hogg, A. E., McMillan, M., Muir, A., & Slater, T. (2018). Net retreat of antarctic glacier grounding lines. *Nature Geoscience*, *11*(4), 258–262.
- Kuipers Munneke, P., Ligtenberg, S. R., Van Den Broeke, M. R., & Vaughan, D. G. (2014). Firn air depletion as a precursor of antarctic ice-shelf collapse. *Journal of Glaciology*, *60*(220), 205–214.

- Lazeroms, W. M., Jenkins, A., Rienstra, S. W., & Van De Wal, R. S. (2019). An analytical derivation of ice-shelf basal melt based on the dynamics of meltwater plumes. *Journal of Physical Oceanography*, *49*(4), 917–939.
- Leguy, G. R., Lipscomb, W. H., & Asay-Davis, X. S. (2021). Marine ice sheet experiments with the community ice sheet model. *The Cryosphere*, *15*(7), 3229–3253.
- Little, C. M., Gnanadesikan, A., & Oppenheimer, M. (2009). How ice shelf morphology controls basal melting. *Journal of Geophysical Research: Oceans*, *114*(C12).
- Martin, M., Winkelmann, R., Haseloff, M., Albrecht, T., Bueler, E., Khroulev, C., & Levermann, A. (2011). The potsdam parallel ice sheet model (pism-pik)–part 2: dynamic equilibrium simulation of the antarctic ice sheet. *The Cryosphere*, *5*(3), 727–740.
- Massom, R. A., Scambos, T. A., Bennetts, L. G., Reid, P., Squire, V. A., & Stammerjohn, S. E. (2018). Antarctic ice shelf disintegration triggered by sea ice loss and ocean swell. *Nature*, *558*(7710), 383–389.
- Mitrovica, J. X., Gomez, N., & Clark, P. U. (2009). The sea-level fingerprint of west antarctic collapse. *Science*, *323*(5915), 753–753.
- Morlighem, M., Rignot, E., Binder, T., Blankenship, D., Drews, R., Eagles, G., . . . others (2020). Deep glacial troughs and stabilizing ridges unveiled beneath the margins of the antarctic ice sheet. *Nature Geoscience*, *13*(2), 132–137.
- Morris, E. M., & Vaughan, D. G. (2003). Spatial and temporal variation of surface temperature on the antarctic peninsula and the limit of viability of ice shelves. *Antarctic Research Series*, *79*(10.1029).
- Pattyn, F., Favier, L., Sun, S., & Durand, G. (2017). Progress in numerical modeling of antarctic ice-sheet dynamics. *Current climate change reports*, *3*(3), 174–184.
- Pattyn, F., Perichon, L., Aschwanden, A., Breuer, B., De Smedt, B., Gagliardini, O., . . . others (2008). Benchmark experiments for higher-order and full-stokes ice sheet models (ismip–hom). *The Cryosphere*, *2*(2), 95–108.
- Pelle, T., Morlighem, M., & Bondzio, J. H. (2019). Brief communication: Picop, a new ocean melt parameterization under ice shelves combining pico and a plume model. *The Cryosphere*, *13*(3), 1043–1049.
- Pfeffer, W. T., Meier, M. F., & Illangasekare, T. H. (1991). Retention of greenland runoff by refreezing: implications for projected future sea level change. *Journal of Geophysical Research: Oceans*, *96*(C12), 22117–22124.
- Pritchard, H., Ligtenberg, S. R., Fricker, H. A., Vaughan, D. G., van den Broeke, M. R., & Padman, L. (2012). Antarctic ice-sheet loss driven by basal melting of ice shelves. *Nature*, *484*(7395), 502–505.

- Reese, R., Albrecht, T., Mengel, M., Asay-Davis, X., & Winkelmann, R. (2018). Antarctic sub-shelf melt rates via pico. *The Cryosphere*, *12*(6), 1969–1985.
- Rignot, E., Mouginot, J., Morlighem, M., Seroussi, H., & Scheuchl, B. (2014). Widespread, rapid grounding line retreat of pine island, thwaites, smith, and kohler glaciers, west antarctica, from 1992 to 2011. *Geophysical Research Letters*, *41*(10), 3502–3509.
- Rignot, E., Mouginot, J., & Scheuchl, B. (2011). Antarctic grounding line mapping from differential satellite radar interferometry. *Geophysical Research Letters*, *38*(10).
- Scambos, T., Fricker, H. A., Liu, C.-C., Bohlander, J., Fastook, J., Sargent, A., . . . Wu, A.-M. (2009). Ice shelf disintegration by plate bending and hydro-fracture: Satellite observations and model results of the 2008 wilkins ice shelf break-ups. *Earth and Planetary Science Letters*, *280*(1-4), 51–60.
- Schoof, C., & Hindmarsh, R. C. (2010). Thin-film flows with wall slip: an asymptotic analysis of higher order glacier flow models. *Quarterly journal of mechanics and applied mathematics*, *63*(1), 73–114.
- Seroussi, H., Nowicki, S., Simon, E., Abe-Ouchi, A., Albrecht, T., Brondex, J., . . . others (2019). initmip-antarctica: an ice sheet model initialization experiment of ismip6. *The Cryosphere*, *13*(5), 1441–1471.
- Shapiro, N. M., & Ritzwoller, M. H. (2004). Inferring surface heat flux distributions guided by a global seismic model: particular application to antarctica. *Earth and Planetary Science Letters*, *223*(1-2), 213–224.
- Shepherd, A., Ivins, E., Rignot, E., Smith, B., Van Den Broeke, M., Velicogna, I., . . . others (2018). Mass balance of the antarctic ice sheet from 1992 to 2017. *Nature*, *558*, 219–222.
- Silvano, A., Rintoul, S. R., & Herraiz-Borreguero, L. (2016). Ocean-ice shelf interaction in east antarctica. *Oceanography*, *29*(4), 130–143.
- Slangen, A., & Haasnoot, M. (2020). Timing of rates and magnitude of sea-level rise projection families. In *Egu general assembly conference abstracts* (p. 13301).
- Smith, J. A., Graham, A. G., Post, A. L., Hillenbrand, C.-D., Bart, P. J., & Powell, R. D. (2019). The marine geological imprint of antarctic ice shelves. *Nature Communications*, *10*(1), 1–16.
- Spergel, J. J., Kingslake, J., Creyts, T., van Wessem, M., & Fricker, H. A. (2021). Surface meltwater drainage and ponding on amery ice shelf, east antarctica, 1973–2019. *Journal of Glaciology*, *67*(266), 985–998.
- Stewart, A. L., Klocker, A., & Menemenlis, D. (2018). Circum-antarctic shoreward heat transport derived from an eddy-and tide-resolving simulation. *Geophysical Research Letters*, *45*(2), 834–845.

- Sun, S., Pattyn, F., Simon, E. G., Albrecht, T., Cornford, S., Calov, R., ... others (2020). Antarctic ice sheet response to sudden and sustained ice-shelf collapse (abumip). *Journal of Glaciology*, 66(260), 891–904.
- Surminski, S., Aerts, J. C., Botzen, W., Hudson, P., Mysiak, J., & Pérez-Blanco, C. D. (2015). Reflections on the current debate on how to link flood insurance and disaster risk reduction in the european union. *Natural Hazards*, 79(3), 1451–1479.
- Trusel, L. D., Frey, K. E., Das, S. B., Karnauskas, K. B., Munneke, P. K., Van Meijgaard, E., & Van Den Broeke, M. R. (2015). Divergent trajectories of antarctic surface melt under two twenty-first-century climate scenarios. *Nature Geoscience*, 8(12), 927–932.
- van Rijswick, H., Gilissen, H. K., Keessen, A., van Doorn-Hoekveld, W., & Wiering, M. (2015). Shifts in floods policies in netherlands.
- Van Wessem, J., Reijmer, C., Morlighem, M., Mouginot, J., Rignot, E., Medley, B., ... others (2014). Improved representation of east antarctic surface mass balance in a regional atmospheric climate model. *Journal of Glaciology*, 60(222), 761–770.
- Van Wessem, J., Van De Berg, W. J., Noël, B. P., Van Meijgaard, E., Amory, C., Birnbaum, G., ... others (2018). Modelling the climate and surface mass balance of polar ice sheets using racmo2–part 2: Antarctica (1979–2016). *The Cryosphere*, 12(4), 1479–1498.